Modeling of "Living" Free-Radical Polymerization Processes. I. Batch, Semibatch, and Continuous Tank Reactors

Min Zhang, W. Harmon Ray

University of Wisconsin–Madison, 1415 Engineering Drive, Madison, Wisconsin 53706

Received 9 October 2001; accepted 9 December 2001

ABSTRACT: A comprehensive mathematical model is developed for "living" free-radical polymerization carried out in tank reactors and provides a tool for the study of process development and design issues. The model is validated using experimental data for nitroxide-mediated styrene polymerization and atom transfer radical copolymerization of styrene and *n*-butyl acrylate. Simulations show that the presence of reversible capping reactions between growing and dormant polymer chains should boost initiation efficiency when using free nitroxide in conjunction with conventional initiator and also increase the effectiveness of thermal initiation. A study shows the effects of the value of the capping equilibrium constant and capping reaction rate constants for both nitroxide-mediated styrene polymerization (using alkoxyamine as polymer chain seeds) and atom transfer radical polymerization of *n*-butyl acrylate (using methyl 2-bromopropionate as chain extension seeds). Also the effect of introducing additional conventional initiator into atom transfer radical polymerization of *n*-butyl acrylate is studied. It is found that the characteristics of long chain growth are determined by the fast exchange of radicals between growing and dormant polymer chains. Polymerization results in batch, semibatch, and a series of continuous tank reactors are analyzed. The simulations also show that a semibatch reactor is most flexible for the preparation of polymers with controlled architecture. For continuous tank reactors, the residence time distribution has a significant effect on the development of chain architecture. J Appl Polym Sci 86: 1630–1662, 2002

Key words: modeling; "living" free-radical polymerization; kinetics; reactor; residence time distribution

INTRODUCTION

In the field of polymer science, the ability to tailor macromolecular structure is one of the primary goals for polymer chemists. Rapid developments in "living" free-radical polymerization[1] have allowed the successful preparation of polymers with tailored polymer chain architectures through a more flexible and versatile route compared to that of anionic polymerization. Living free-radical polymerization combines the advantages of free-radical chemistry and living polymerization capabilities. Free-radical chemistry can polymerize most monomers and it can better tolerate impurities such as water and oxygen. For example, living free-radical polymerization makes possible the production of some functional polymers [e.g. poly(vinyl acetate)] that cannot be achieved by any other methods, and with narrow molecular weight distributions.[2] Furthermore, heterogeneous polymerizations such as emulsion polymerization, suspension polymerization, and dispersion polymerization[3–5] can also be used so that it is possible to produce polymers with predetermined molecular architecture and with well-controlled particle morphology.

There is a large literature on the chemistry of living free-radical polymerization. However, most work focuses on finding new agents to convert a conventional free-radical polymerization system into a "living" one. The earlier living free-radical polymerization systems consist of nitroxide-mediated radical polymerization[1] and atom transfer radical polymerization (ATRP).[6] In a nitroxide-mediated radical polymerization system, nitroxide radicals reversibly cap the growing radicals to form a dormant species. By contrast, ATRP is based on the reversible formation of radicals from alkyl halides and similar agents, and is accompanied by the redox process under a transition metal catalyst. These two cases directly introduce reversible reactions between growing and dormant chains.

More recently, other approaches, such as reversible addition fragmentation chain transfer (RAFT) radical polymerization show living polymerization features.[7–11] Sawamoto and coworkers[12] suggest that living free-radical polymerization in aqueous suspensions should behave similarly to bulk polymerization. Some workers[4,13–15] have studied living free-radical polymerization in emulsion and miniemulsion reactors and suggest that this may be the most effective process for high reaction rates and close control of molecular architecture.

Although research to clarify the mechanism of living free-radical polymerization is still proceeding,

Correspondence to: W. Ray (ray@engr.wisc.edu).
Contract grant sponsor: National Science Foundation.

Journal of Applied Polymer Science, Vol. 86, 1630–1662 (2002)

TABLE I
"Living" Free-Radical Polymerization Mechanisms

Initiation	
Initiator	$I \xrightarrow{fk_{iniid}} 2P_0$
Reversible reaction of primary capped species	$P_0 + CAP \overset{k_{cappri}}{\rightleftharpoons}$ PriCapped $(+ CAT)$
Special initiation	$y(i)M_i \xrightarrow{k_{spinii}} x(i)P_{\boldsymbol{\delta}_i,i}$
Chain initiation	$P_0 + M_i \xrightarrow{k_{pi}} P_{\boldsymbol{\delta}_i,i}$
Propagation	$P_{\mathbf{n},j} + M_i \xrightarrow{k_{pij}} P_{\mathbf{n}+\boldsymbol{\delta}_i,i}$
Chain transfer	
to solvent	$P_{\mathbf{n},j} + S \xrightarrow{k_{ctsj}} D_{\mathbf{n}} + S\cdot$
to agent	$P_{\mathbf{n},j} + CTA \xrightarrow{k_{ctCTAj}} D_{\mathbf{n}} + CTA\cdot$
to monomer	$P_{\mathbf{n},j} + M_i \xrightarrow{k_{ctMij}} D_{\mathbf{n}} + P_{\boldsymbol{\delta}_i,i}$
spontaneous	$P_{\mathbf{n},j} \xrightarrow{k_{ctspj}} D_{\mathbf{n}} + H\cdot$
Reinitiation	$S\cdot, CTA\cdot; H\cdot + M_i \xrightarrow{k_{pi}} P_{\boldsymbol{\delta}_i,i}$
Reversible capping reaction	$P_{\mathbf{n},j} + CAP \overset{k_{cappj}}{\rightleftharpoons} Q_{\mathbf{n},j}(+ CAT)$
Degenerative reaction	$P_{\mathbf{n},j} + Q_{\mathbf{m},i} \overset{k_{cdij}}{\rightleftharpoons} P_{\mathbf{m},i} + Q_{\mathbf{n},j}$
Chain termination	
by inhibitor	$P_{\mathbf{n},j} + X \xrightarrow{k_{txj}} D_{\mathbf{n}}$
	$P_0 + X \xrightarrow{k_{tx}}$ fragments
by disproportionation	$P_{\mathbf{n},j} + P_{\mathbf{m},i} \xrightarrow{k_{tdij}} D_{\mathbf{n}} + D_{\mathbf{m}}$
by combination	$P_{\mathbf{n},j} + P_{\mathbf{m},i} \xrightarrow{k_{tcij}} D_{\mathbf{m}+\mathbf{n}}$
Decomposition of dormant species	$Q_{\mathbf{n}} \xrightarrow{k_{decomj}} D_{\mathbf{n}} +$ fragments

there has been some work on the modeling of the kinetics of these living free-radical polymerization processes. Yan et al.[16] developed a simple kinetic model for living free-radical polymerization, discussing the effects of propagation and capping rate constants and reactant concentrations on polydispersity. Veregin et al.[17] presented a general solution for the molecular weight distribution as a function of conversion in nitroxide-mediated styrene free-radical polymerization, considering that the initiation is instantaneous and the termination reaction is negligible. They concluded that the polydispersity in this system is

TABLE II
General Polymer Chain and Moment Definitions

$P_{\mathbf{n},j} \equiv$ A growing polymer chain with n_i monomer units of type i and end groups of type j
$Q_{\mathbf{n},j} \equiv$ A dormant polymer chain with n_i monomer units of type i and end groups of type j
$D_{\mathbf{n}} \equiv$ A dead polymer chain with n_i monomer units of type i
Growing polymer moments
$\mu_{\mathbf{f},j} \equiv \sum_{\mathbf{n}=1}^{\infty} \mathbf{n}^{\mathbf{f}} P_{\mathbf{n},j}$
Dormant polymer moments
$\nu_{\mathbf{f},j} \equiv \sum_{\mathbf{n}=1}^{\infty} \mathbf{n}^{\mathbf{f}} Q_{\mathbf{n},j}$
Live polymer moments
$\zeta_{\mathbf{f},j} = \mu_{\mathbf{f},j} + \nu_{\mathbf{f},j}$
Bulk polymer moments
$\lambda_{\mathbf{f}} \equiv \sum_{\mathbf{n}=1}^{\infty} \mathbf{n}^{\mathbf{f}} [\sum_{j=1}^{N_{mon}} (P_{\mathbf{n},j} + Q_{\mathbf{n},j}) + D_{\mathbf{n}}]$

TABLE III
Calculation of Average Polymer Properties and Conversion

Number-average chain length for bulk polymer	$DP_n = \dfrac{\sum_{i=1}^{N_{mon}} \lambda_{\boldsymbol{\delta}_i}}{\lambda_0}$
Number-average chain length for live polymer	$LDP_n = \dfrac{\sum_{i=1}^{N_{mon}} \xi_{\boldsymbol{\delta}_i}}{\xi_0}$
Number-average chain length for growing polymer	$GDP_n = \dfrac{\sum_{i=1}^{N_{mon}} \mu_{\boldsymbol{\delta}_i}}{\mu_0}$
Weight-average chain length for bulk polymer	$DP_w = \dfrac{\lambda_2}{\sum_{i=1}^{N_{mon}} \lambda_{\boldsymbol{\delta}_i}}$
Polydispersity index for bulk polymer	$Z_p = \dfrac{\lambda_2 \lambda_0}{(\sum_{i=1}^{N_{mon}} \lambda_{\boldsymbol{\delta}_i})^2}$
Mole fraction of bulk polymer that is live	$LX_p = \dfrac{\xi_0}{\lambda_0}$
Mole fraction of live polymer that is growing	$GX_p = \dfrac{\sum_{j=1}^{N_{mon}} \mu_{0,j}}{\xi_0}$
Bulk polymer composition (mole fraction)	$F_p(j) = \dfrac{\lambda_{\boldsymbol{\delta}_j}}{\sum_{i=1}^{N_{mon}} \lambda_{\boldsymbol{\delta}_i}}$
Live polymer composition (mole fraction)	$LF_p(j) = \dfrac{\xi_{\boldsymbol{\delta}_j}}{\sum_{i=1}^{N_{mon}} \xi_{\boldsymbol{\delta}_i}}$
Growing polymer composition (mole fraction)	$GF_p(j) = \dfrac{\mu_{\boldsymbol{\delta}_j}}{\sum_{i=1}^{N_{mon}} \mu_{\boldsymbol{\delta}_i}}$
Growing polymer end-group mole fraction	$F_{eg}(j) = \dfrac{\mu_{0,j}}{\sum_{i=1}^{N_{mon}} \mu_{0,i}}$
Conversion of monomer to polymer	$X_p = \dfrac{\sum_{i=1}^{N_{mon}} \lambda_{\boldsymbol{\delta}_i} MW(i)}{\sum_{i=1}^{N_{mon}} (C_{Mi} + \lambda_{\boldsymbol{\delta}_i}) MW(i)}$

controlled by the exchange rate between the growing and dormant polymer chains. Greszta and Matyjaszewski[18] proposed a detailed kinetic model for 2,2,6,6-tetramethypiperidinyl-1-oxy (TEMPO)-mediated styrene polymerization and estimated the kinetic and thermodynamic parameters for the reversible reaction between growing and dormant species. Fukuda et al.[19] conducted computer simulations for nitroxide-mediated styrene polymerization, concluding that thermal initiation is important in maintaining a reasonable polymerization rate in this system. Fischer[20] presented a kinetic analysis to address the persistent radical effect in living free-radical polymerization. Shipp and Matyjaszewski[21,22] studied styrene ATRP through a kinetic model. They found that termination is subject to diffusional control, which may conceal the persistent radical effect. The apparent external orders of reactants in this system were also studied. Ziegler and Matyjaszewski[23] studied atom transfer radical copolymerization of MMA and *n*-butyl acrylate and used simulations to explain the observed results. Butté et al.[24] developed a general kinetic model for living free-radical polymerization. They assessed the model reliability by comparing simulations to experimental data for TEMPO-mediated

TABLE IV
Styrene Polymerization in the Presence of Alkoxyamine: Operating Conditions

$[Alkoxyamine]_0$	Temperature	Data source
0.012mol/L	120°C	Greszta et al.[18]
0.020mol/L	125°C	Tsujii et al.[19,40]

styrene polymerization and styrene ATRP. They found their model a useful tool for analyzing living free-radical polymerization processes. Zhu[25] presented a kinetic model for stable free-radical polymerization. He discussed the effects of a variety of kinetic parameters and reactant concentrations on polymerization rate and polymer property development. In contrast to deterministic models, He et al.[26] used a Monte Carlo method to study the kinetics and chain length distribution for living free-radical polymerization. The effects of experimental variables, such as initiation rate constant, were explored.

Even though those models have provided insight into what occurs in a "living" free-radical polymerization system, there is still the need for a kinetic model that incorporates a general "living" free-radical polymerization scheme and that can be used to compare different kinetic approaches and to study the effects of reactor engineering. In this study we develop such a model for "living" free-radical multicomponent copolymerization. The model can be used to study the effects of kinetic parameters such as the equilibrium constant and capping reaction, propagation, and termination rate constants on the development of polymer properties. Then it can be used to choose an appropriate reactor type and the best operating conditions for polymerization.

Existing models[16–25] reported in the literature are limited to specific kinetic modeling and, therefore, are not a general tool for designing a practical process. It is often difficult to quantitatively understand how the reactor environment [e.g the residence time and its distribution, operation mode (batch, semibatch, continuous stirred tank reactor, etc.)] influences the development of polymer properties. However, this issue is of great industrial importance for practical polymer production. In this study a comprehensive kinetic

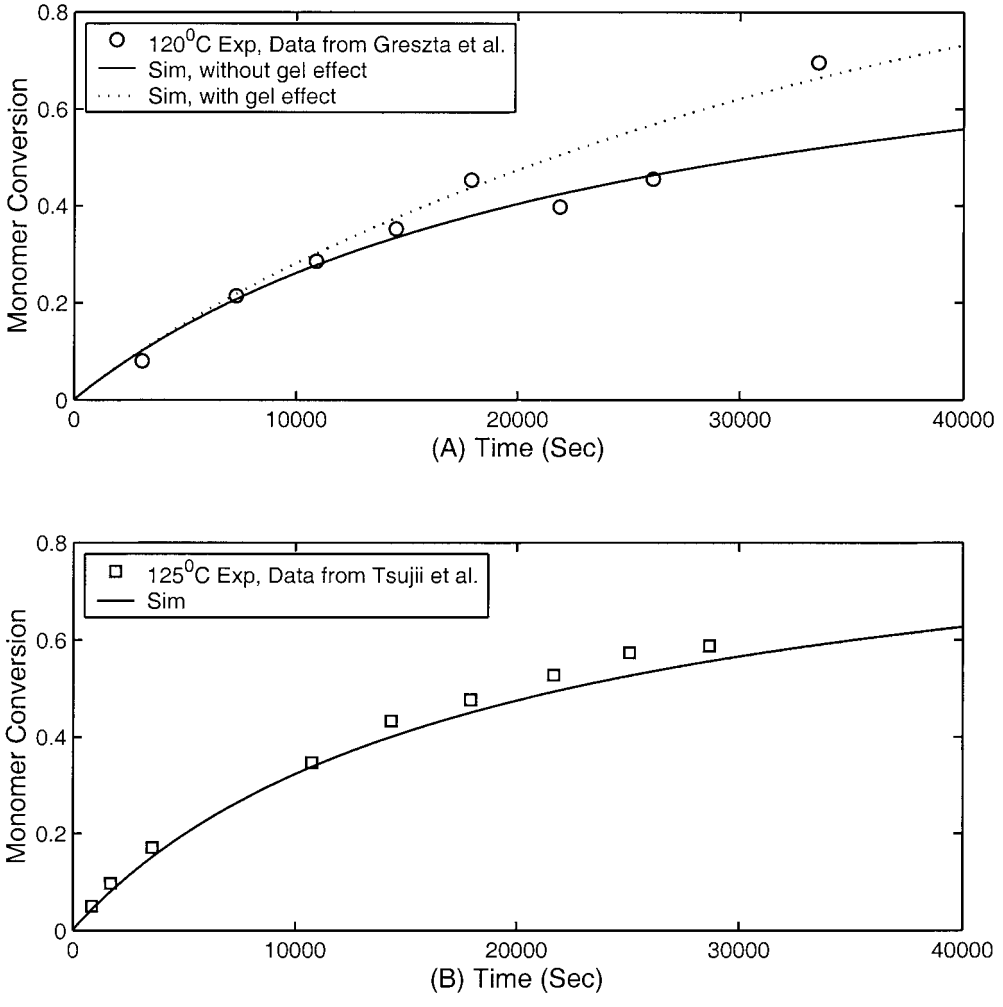

Figure 1 Comparison of model predictions of monomer conversion with experimental data for styrene polymerization in the presence of alkoxyamine. Experimental data from (A) Greszta et al.[18] and (B) Tsujii et al.[19,40]

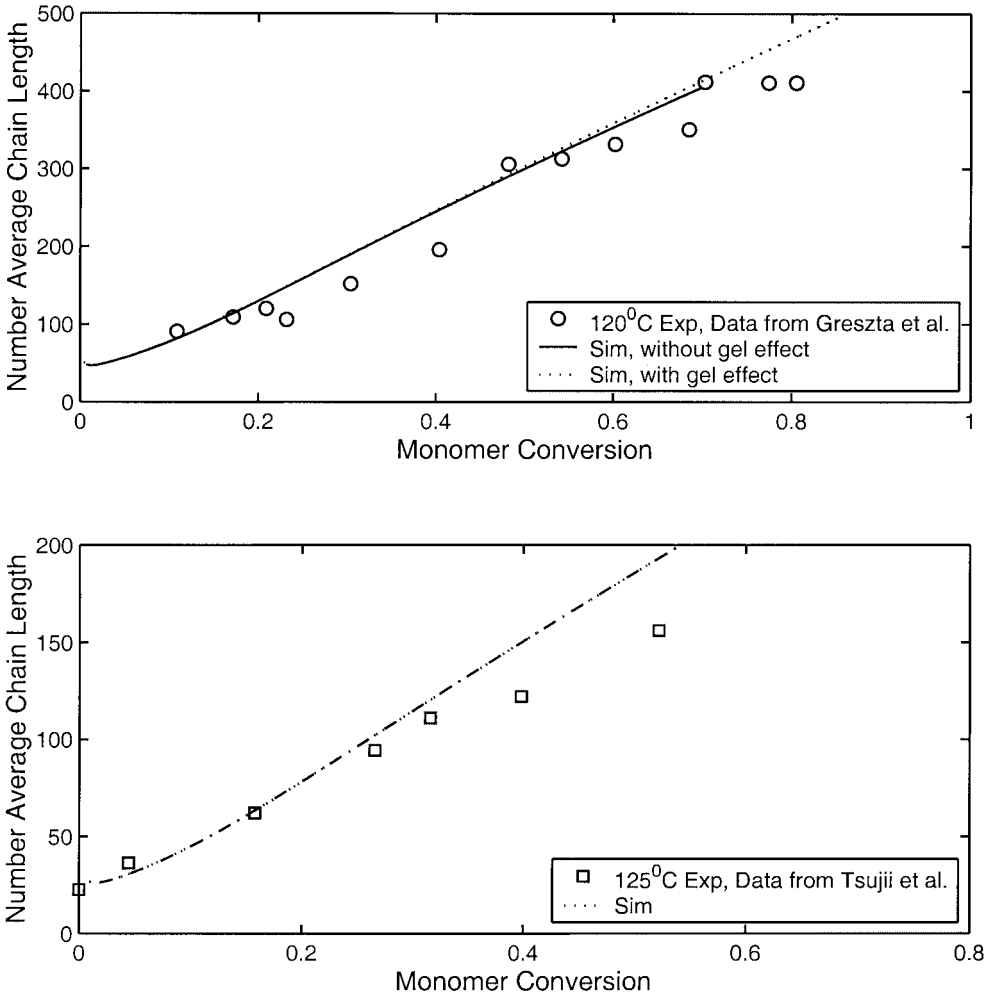

Figure 2 Comparison of model predictions of number-average chain length with experimental data for styrene polymerization in the presence of alkoxyamine. Experimental data from (A) Greszta et al.[18] and (B) Tsujii et al.[19,40]

model is combined with a tank reactor model. Batch, semibatch, and continuous tank reactor (CSTR) processes are conducted for both homopolymerization and copolymerization. To validate the model, we perform case studies of both TEMPO-mediated styrene polymerization and atom transfer radical copolymerization of styrene and *n*-butyl acrylate in batch reactors, comparing model results to experimental data available in the literature. Then, we illustrate the applications of the model to product and process design.

KINETIC MODEL

A general kinetic model for free-radical polymerization involving a reversible reaction between growing and dormant species that results in "living" free-radical polymerization is formulated in detail, as shown in Appendix A. A corresponding module based on this model has been integrated into a POLYRED™ polymerization simulator developed at the University of Wisconsin at Madison. The principal mechanisms of "living" free-radical polymerization are summarized in Table I. As shown in Table II, the reaction system contains three kinds of polymer species: the growing polymer $P_{\mathbf{n},j}$, the dormant polymer $Q_{\mathbf{n},j}$, and the dead polymer $D_{\mathbf{n}}$, where the vector **n** indicates the composition of the polymer and the index j indicates the monomer type of the end group. Furthermore, all moments are defined in Table II according to the method of moments.[27] The moment equations combined with the mass balance equations of all species in the reaction system form the fundamental equations of this model.

The average polymer properties can be calculated using the moments, and the results are summarized in Table III.

Gel effect

Diffusion limitations at high conversions lead to a dramatic decrease in the termination rate, resulting in an autoacceleration of the polymerization in a conventional free-radical polymerization system, a phenom-

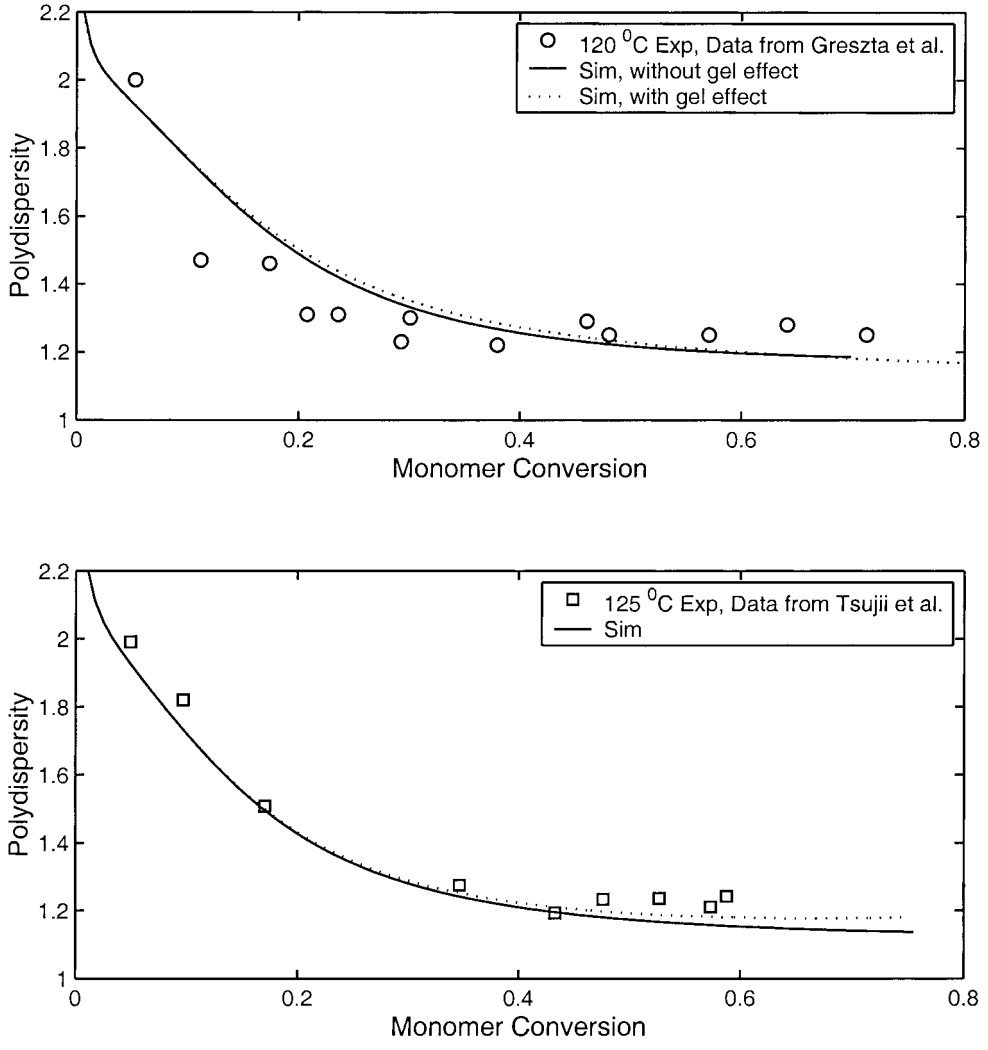

Figure 3 Comparison of model predictions of polydispersity with experimental data for styrene polymerization in the presence of alkoxyamine. Experimental data from (A) Greszta et al.[18] and (B) Tsujii et al.[19,40]

enon known as the Tromsdorff or gel effect. The way that polymer chains extend in a "living" free-radical polymerization is quite different from that in a conventional one. In the conventional system, polymer chains instantaneously approach a high value, normally surpassing the chain entanglement threshold around 100, as suggested by De Gennes.[28] The gel effect becomes important in such a system when polymer mass is high. By contrast, in "living" free-radical polymerization, polymer chains extend steadily from short chains to long chains, and the chain lengths may never surpass the entanglement threshold, so that the gel effect may not be important. However, if the polymer chains indeed are long enough, and polymer mass in the reactor is sufficiently high, the gel effect can then affect polymerization behavior. In this study we consider that, if the number-average polymer chain length is above 150, the gel effect correlation will be used. For the simulations presented in this research, we will point out whether the gel effect is either significant or insignificant. Several gel effect correlations, some empirical and others semiempirical, have appeared in the literature. In this study an empirical correlation for styrene polymerization by Hamer et al.[29] is used.

REACTOR MODEL

In this section, a tank reactor model is developed for "living" free-radical polymerization chemistry, aiming to describe batch, semibatch, and continuous stirred tank reactors (CSTR). The model equations are shown as follows.

Overall mass balance equation

A total material balance around the well-mixed reactor yields

$$\frac{d(V\rho)}{dt} = Q_f\rho_f - Q_o\rho \tag{1}$$

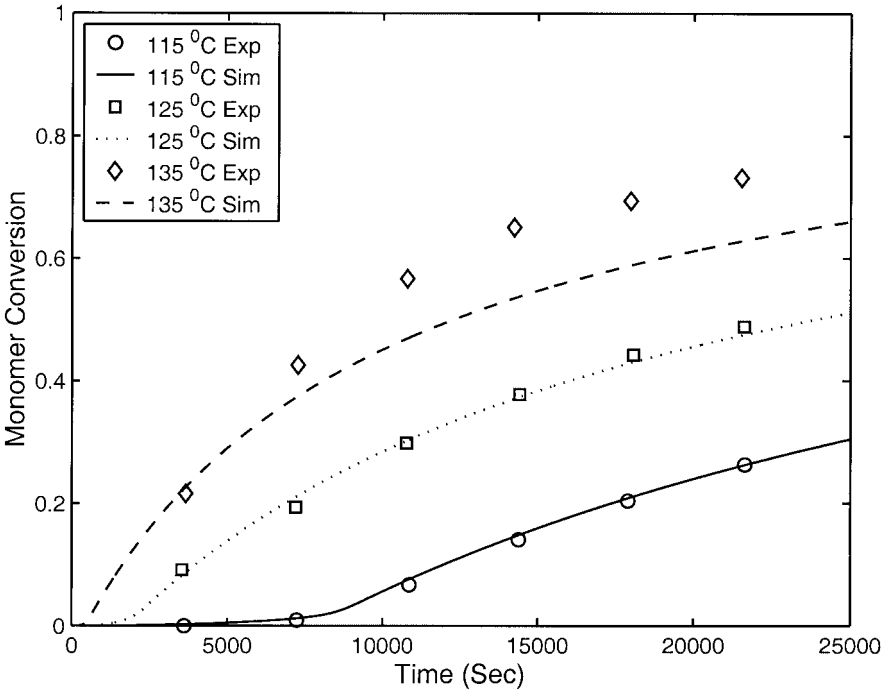

Figure 4 Comparison of model predictions of conversion with experimental data for TEMPO-mediated polymerization of styrene at the temperatures of 115, 125, and 135°C, respectively, with $[BPO]_0 = 0.036$ mol/L and [TEMPO]/[BPO] = 1.1:1. Experimental data from Georges et al.[17,33]

that is,

$$\frac{dV}{dt} = \frac{Q_f \rho_f}{\rho} - Q_o - \frac{V}{\rho}\frac{d\rho}{dt} \tag{2}$$

Monomer conversion X_P is defined as the fraction of monomer units converted into polymer over the total amount of monomer units in the reactor, which includes monomers and all polymers.

$$X_P = \frac{\lambda_1}{\lambda_1 + C_M} \tag{3}$$

Mass balance equation for generic species *i*

The mass balance equation for generic species i, in a tank reactor, can be written as

$$\frac{d}{dt}(VC_i) = Q_f C_{if} - Q_o C_i + V R_{C_i} \tag{4}$$

that is,

$$\frac{dC_i}{dt} = \frac{1}{V}\left[Q_f C_{if} - \left(Q_o + \frac{dV}{dt}\right)C_i\right] + R_{C_i} \tag{5}$$

where

$$C_i = C_S, C_{CTA}, C_X, C_I, C_{\text{PriCapped}}, C_{CAT}, C_{CAP}, C_{M_i}, C_{P_0},$$
$$\mu_{0,j}, \mu_{\delta_k}, \nu_{0,j}, \nu_{\delta_k}, \lambda_0, \lambda_{\delta_k}, \lambda_2$$

Energy balance equation

The general energy balance equation for a tank reactor is

$$\frac{d(V\rho e)}{dt} + C\frac{dT}{dt} = Q_f \rho_f e_f - Q_o \rho e - U_j A_j (T - T_j) - U_a A_a (T - T_a) + V e_{rxn} + E_{\text{input}} \tag{6}$$

$$e = \int_{T_{ref}}^{T} C_p \, dT \tag{7}$$

in which C is the reactor wall heat capacity, e is the enthalpy density of the reactant mixture, U_j is the overall heat transfer coefficient for the jacket, and U_a is the overall heat transfer coefficient for the reactor with respect to the ambient environment.

Calculation of physical properties

Pure component densities and heat capacities in this work are considered as polynomial functions of reactor temperature.

Assume that the mixture density ρ is a function of temperature and component concentrations [i.e., $\rho = \rho(T, C_i)$] and volume additivity holds [i.e., $1/\rho = \Sigma_i(w_i/\rho_i^0)$], in which ρ_i^0 denotes the density of pure component i and w_i is the weight fraction of component i; then,

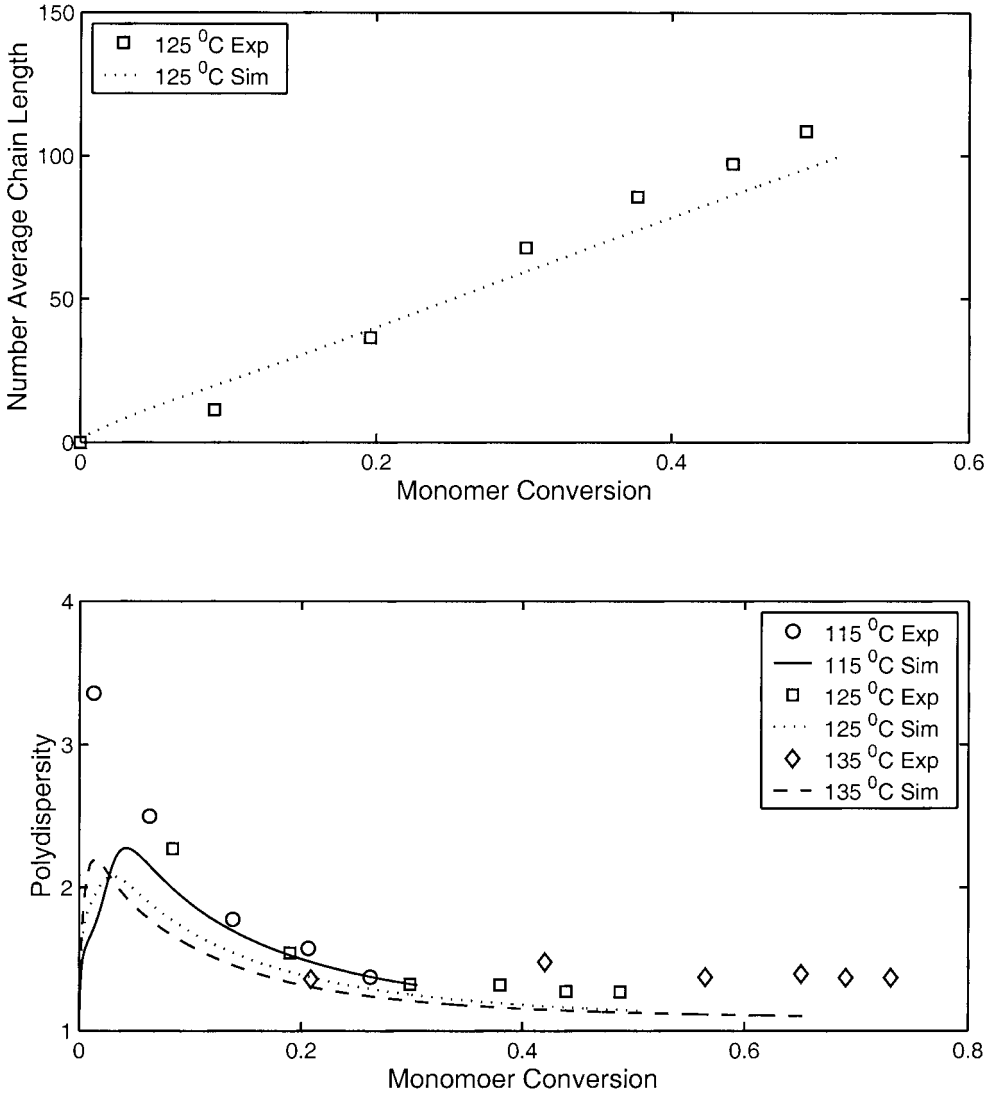

Figure 5 Comparison of model predictions of polydispersity with experimental data for TEMPO-mediated polymerization of styrene at the temperatures of 115, 125, and 135°C, respectively, with $[BPO]_0 = 0.036$ mol/L and [TEMPO]/[BPO] = 1.1:1. Experimental data from Georges et al.[17,33]

$$\frac{d\rho}{dt} = \frac{\partial \rho}{\partial T}\frac{dT}{dt} + \sum_i \frac{\partial \rho}{\partial C_i}\frac{dC_i}{dt}$$

$$= \rho^2 \frac{dT}{dt}\sum_i \frac{w_i}{(\rho_i^0)^2}\frac{d\rho_i^0}{dT} + \sum_i \left(1 - \frac{\rho}{\rho_i^0}\right) M w_i \frac{dC_i}{dt} \quad (8)$$

Similarly, the mixture heat capacity c_p is assumed a function of temperature and concentrations [i.e., $c_p = c_p(T, C_i)$] and mass additivity for mixture capacity holds (i.e., $c_p = \Sigma_i w_i c_{pi}^0$, in which c_{pi}^0 denotes the capacity of component i.

MODEL VALIDATION

"Living" free-radical polymerization systems have been extensively studied experimentally in the past several years. Among them, TEMPO-mediated styrene polymerization and atom transfer radical copolymerization of styrene and *n*-butyl acrylate in the presence of copper salt are chosen as model systems to validate the model in this study because of the availability of data in the literature and their potential for industrial application.

TEMPO-mediated styrene polymerization

Polymerization of styrene in the presence of stable radicals, 2,2,6,6-tetramethypiperidinyl-1-oxy (TEMPO), or TEMPO-terminated initiator (alkoxyamines) shows typical "living" free-radical polymerization features,[1,19,30–34] given that polymer chain length increases linearly with respect to monomer conversion and the polymers produced have very narrow molecular weight

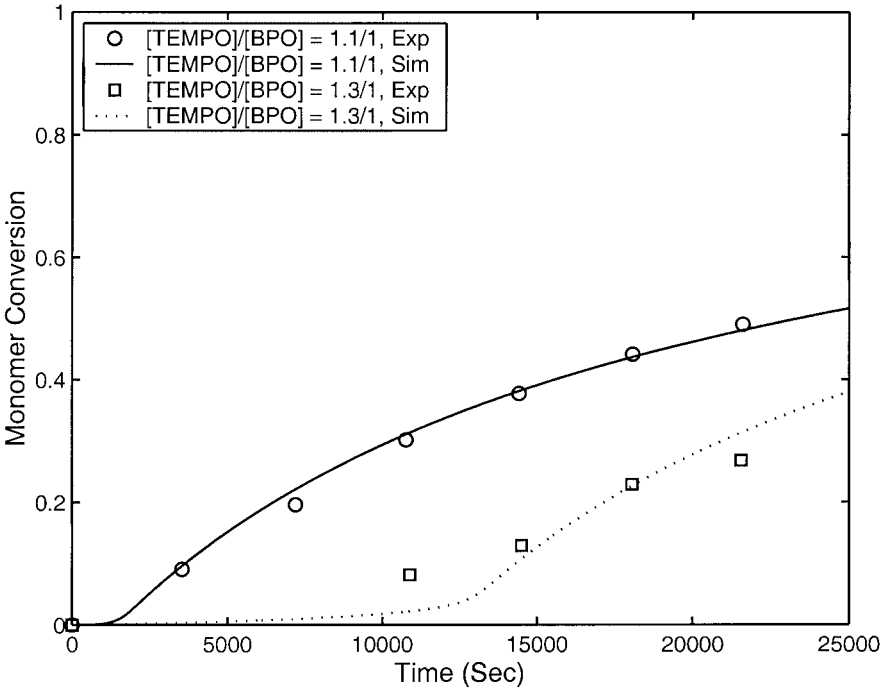

Figure 6 Comparison of model predictions of monomer conversion with experimental data for TEMPO-mediated polymerization of styrene at 125°C, with $[BPO]_0$ = 0.036 mol/L and [TEMPO]/[BPO] = 1.1:1 (initiation efficiency is 0.54) and [TEMPO]/[BPO] = 1.3:1 (initiation efficiency is 0.62). Experimental data from Georges et al.[17,33]

distributions. Early reports of the use of TEMPO and alkoxyamines in free-radical polymerization were from Rizzardo and Solomon[35,36] for the preparation of oligomers using a variety of monomers, and from Georges et al.[1,17,32,33] for longer chain polymerization. Kinetic data of styrene polymerization in the presence of TEMPO have been reported from several groups[17–19,30,33] and provide a good basis for validating the model proposed in this work. These experiments were conducted under various conditions: (i) different TEMPO concentrations, (ii) with or without a conventional initiator, and (iii) different temperatures.

For our validation studies, a kinetic scheme is assumed that includes reversible capping reactions between growing and dormant polymer chains, thermal initiation of styrene, propagation, termination, and conventional initiation if initiator is used. Although it has also been reported that the dormant polymer chains may experience a side reaction/thermal decomposition to form dead polymer, in our work we found this mechanism to have a negligible effect on monomer conversion and polymer properties. For more details, see Zhang.[37]

All kinetic parameters and their sources can be found in Appendix B. Note that the reaction of any nitroxide with a sterically unhindered radical is very fast and the rate constant shown is chosen in the range reported by several workers.[18,19,38,39] The role of thermal initiation in this system has been debated. Georges et al.[17] suggest that the effect of thermal initiation and bimolecular termination can be neglected at temperatures below 115°C. By contrast, Matyjaszewski et al.,[18] Fukuda et al.,[19,40] and Devonport et al.[30] reported that thermal initiation plays a key role in maintaining a reasonable polymerization rate in this system. To be consistent with these findings, thermal initiation is considered in our simulations shown below.

Styrene polymerization in the presence of alkoxyamine

Greszta et al.[18] and Fukuda et al.[19,40] studied styrene polymerization independently by using alkoxyamines as initiator. Alkoxyamines are formed by either reacting peroxides and/or diazo initiators with the corresponding nitroxyl radicals or reacting a large amount of nitroxyl radicals with monomers that can be thermally initiated, such as styrene. This methodology permits the introduction of a specified number of polymer chains into the system and allows for better control of polymer chain architecture over those formed *in situ*.[30] Experimental conditions for the data are listed in Table IV.

Figures 1, 2, and 3 show the development of monomer conversion and properties of polymer chains with respect to time. The model predictions agree very well with the shorter chain length data from Tsujii et al.,[40] without considering the gel effect [Fig. 1(B)]. By contrast, the number-average chain length is above 200 in the system of Greszta et al.[18] when the monomer conversion is only 40%; therefore, simulations both

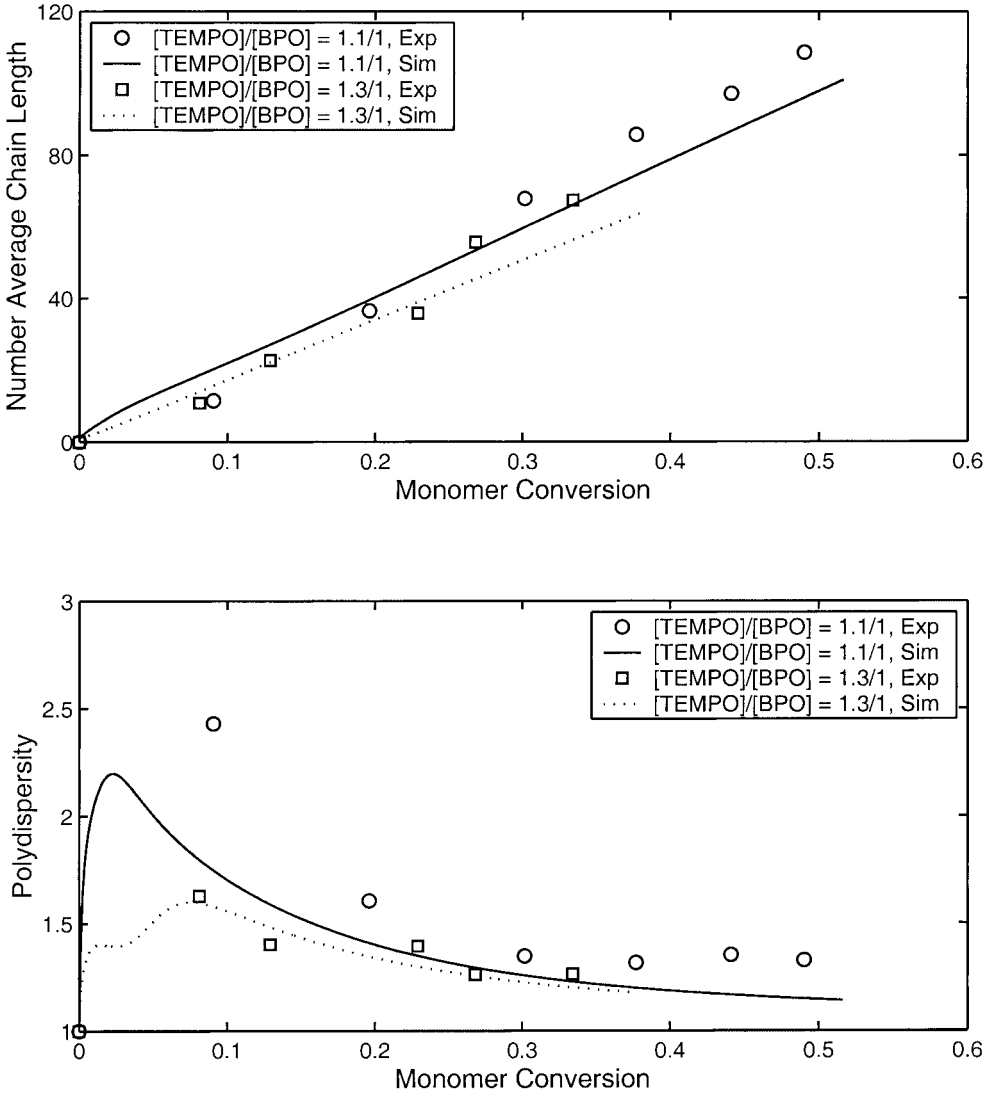

Figure 7 Comparison of model predictions of number-average chain length and polydispersity with experimental data for TEMPO-mediated polymerization of styrene at 125°C, with $[BPO]_0$ = 0.036 mol/L and [TEMPO]/[BPO] = 1.1:1 (initiation efficiency is 0.54) and [TEMPO]/[BPO] = 1.3:1 (initiation efficiency is 0.62). Experimental data from Georges et al.[17,33]

with and without gel effect are presented. The overall predictions of the data of Greszta et al. are reasonably good, but there is too much scatter in the data to determine whether the gel effect is necessary. The important point is that the kinetic model, with parameters taken from the literature, is in good agreement with experimental data from two different laboratories.

Styrene polymerization in the presence of benzoyl peroxide and TEMPO

Polymerization of styrene in the presence of benzoyl peroxide (BPO) and TEMPO was investigated by Georges et al.[17,33] Experiments were reported at temperatures of 115, 125, and 135°C, with the initial ratio [TEMPO]/[BPO] = 1.1/1. When using a conventional initiator, the initiator efficiency f has to be determined. The typical value of initiator efficiency for BPO ranges from 0.5 to 0.6, and in this simulation, the values of 0.54, 0.544, and 0.546 are used for 115, 125, and 135°C, respectively. The introduction of TEMPO may have a significant impact on initiator efficiency, as discussed in a later paragraph. Figure 4 shows model predictions and experimental conversion profiles versus time. At 115°C, there is a pronounced induction period, which decreases at higher reactor temperatures. Thus, predicting this effect is a good demonstration of our model fidelity. The controlling mechanism is as follows: initially, the TEMPO concentration is quite high, causing TEMPO to cap radicals from the decomposition of initiator, and leading to alkoxyamine formation *in situ*. At 135°C, the decomposition of BPO is extremely fast and generates radicals that are capped by TEMPO immediately; hence, the concentration of TEMPO drops quickly to a small stationary value. The resulting concentration of active radicals is adequate

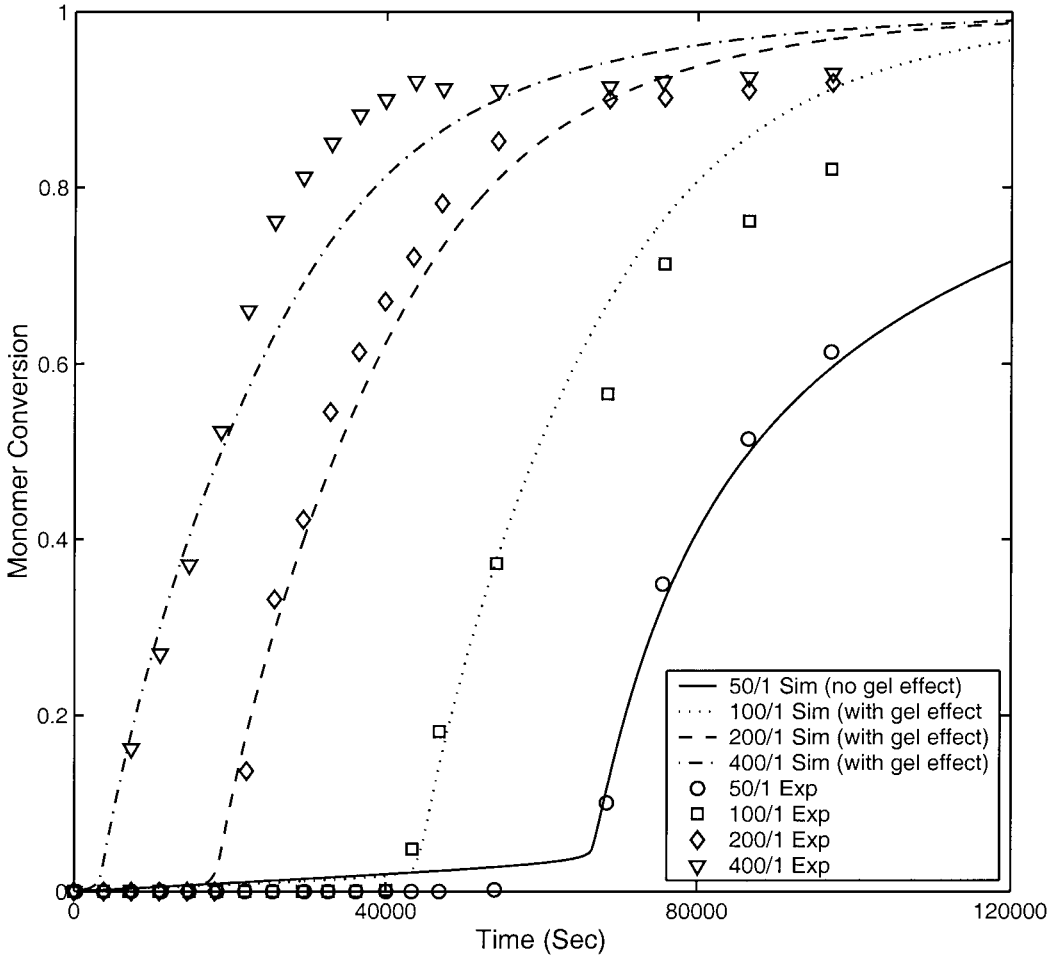

Figure 8 Conversion with respect to time in styrene thermal polymerization in the presence of TEMPO at 125°C: comparison of simulations and experimental observations. Note that the ratio in the figure denotes the ratio of styrene with respect to TEMPO. Experimental data from Devonport et al.[30]

to immediately begin polymerization. By contrast, at 115°C, the much slower rate of generation of radicals from BPO decomposition becomes the controlling step for initiation of polymerization and it takes a much longer time for the TEMPO concentration to decrease by the capping reaction. Thus the concentration of active radicals is very low for a long time, delaying the onset of polymerization. Figure 5 shows that polymer chain length increases linearly as a function of conversion and the resulting polymers also have narrow molecular weight distributions.

TABLE V
Adjustment of Thermal Initiation Rate Constant for Styrene Thermal Polymerization in the Presence of TEMPO[a]

[St]/[TEMPO]	k_{spini} (L^2 mol^{-2} s^{-1}) at 125°C
50/1	2.418×10^{-9}
100/1	1.900×10^{-9}
200/1	2.245×10^{-9}
400/1	8.636×10^{-9}

[a] Note that the normal thermal initiation rate constant, $k_{spini} = 1.891 \times 10^{-10}$ L^2 mol^{-2} s^{-1} at 125°C, is reused after the concentration of free TEMPO drops to a stationary value (on the order of 1×10^{-4} mol/L).

Because the induction period should be dependent on the balance between rate of free-radical generation and TEMPO concentration, it is possible to create an induction period by adding excess TEMPO. Georges et al.[17,33] studied the role of excess TEMPO by varying the initial ratio of [TEMPO]/[BPO] from 1.1/1 to 1.3/1 at 125°C. Figure 6 shows model predictions compared to experimental conversion curves for the two different levels of TEMPO. Note that at the higher TEMPO level, the induction period becomes very significant, as predicted by the model. Similar observations have been found in both experiment and simulation by Butté et al.[24] for styrene polymerization in the presence of AIBN and TEMPO. In their simulations, they found that the initiator efficiency of AIBN is not constant, increasing from 0.56 to 0.725 when the initial ratio of [TEMPO]/[AIBN] increases from 1.1 to 1.5. In our simulations, the initiator efficiencies are chosen to be 0.54 for [TEMPO]/[BPO] = 1.1/1 and 0.62 for [TEMPO]/[BPO] = 1.3/1. It seems that the increase of TEMPO concentration improves the initiator effi-

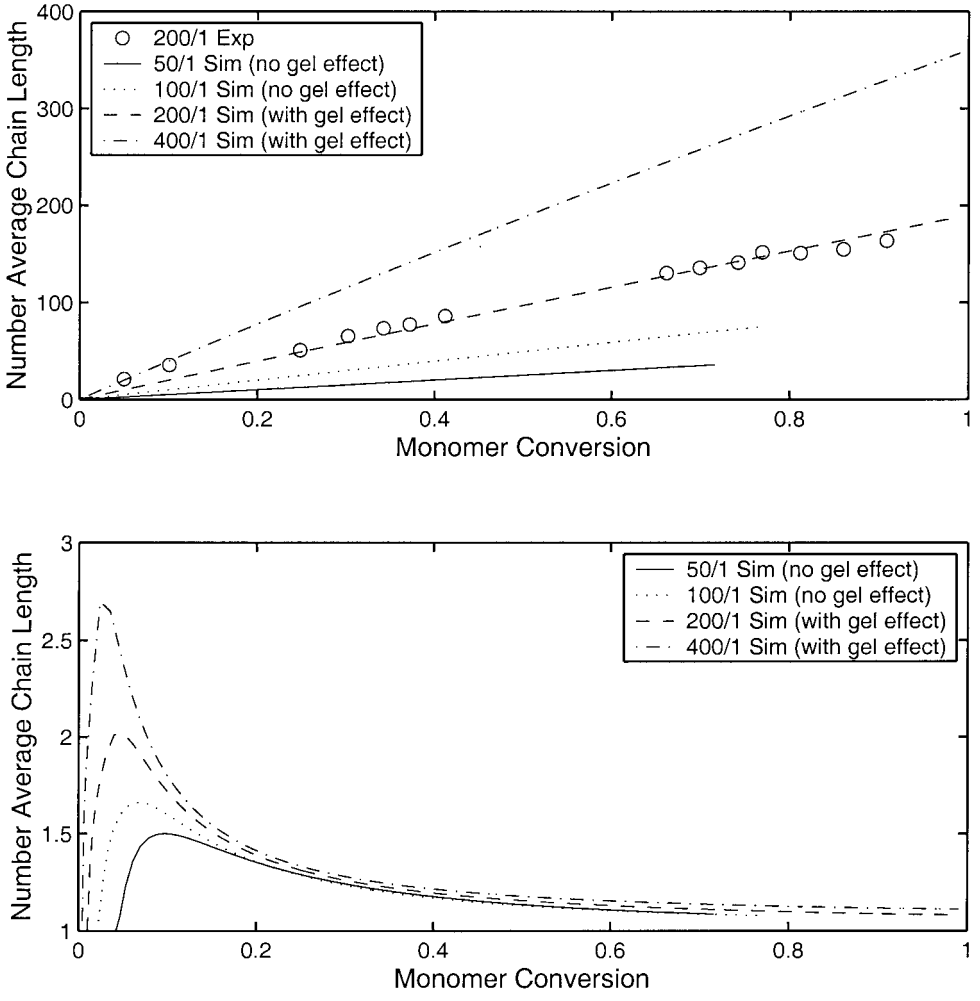

Figure 9 Dependency of number-average chain length and polydispersity on monomer conversion in styrene thermal polymerization in the presence of TEMPO at 125°C. Experimental data from Devonport et al.[30]

ciency. In a conventional free-radical polymerization, various side reactions such as the cage reaction of the primary radicals from initiator, primary radical termination, and other reactions may lead to the loss of effective radicals. When TEMPO is added, the capping reaction of TEMPO with primary radicals is so fast that the other side reactions are limited and the initiator efficiency is increased. However, a better understanding of these phenomena is needed so that it is possible to have *a priori* prediction of initiator efficiency as a function of temperature and TEMPO concentration. A first attempt is shown in Appendix C.

Figure 7 shows the evolution of the resulting polymer chain length and polydispersity in the reactor. Under both [TEMPO]/[BPO] ratios, the polymer chains are extended linearly with respect to conversion and have a very narrow molecular weight distribution.

Again, the model has been able to predict the experimental data for styrene polymerization in the presence of TEMPO and BPO reasonably well, and in particular to explain observed induction periods.

Styrene thermal polymerization in the presence of TEMPO

Devonport et al.[30] carried out experiments to investigate the role of thermal initiation in TEMPO-mediated styrene polymerization. A solution of TEMPO in styrene was heated at 125°C for over 20 h. Samples of the polymerization mixture were taken periodically to measure monomer conversion, molecular weight, and the MWD. Figure 8 shows a comparison of model simulations to their experimental observations for conversion. A very significant induction period appears during the polymerization and depends on the concentration of TEMPO. The mechanism is similar to that for the case of chemical initiation. Radicals generated by thermal initiation are rapidly capped by TEMPO, thus preventing polymerization from proceeding until almost all of the TEMPO is consumed. Once a low level of TEMPO concentration is reached, the concentration of growing radicals is high enough to allow polymerization.

The effectiveness of thermal initiation is also greatly increased by the presence of TEMPO because the rad-

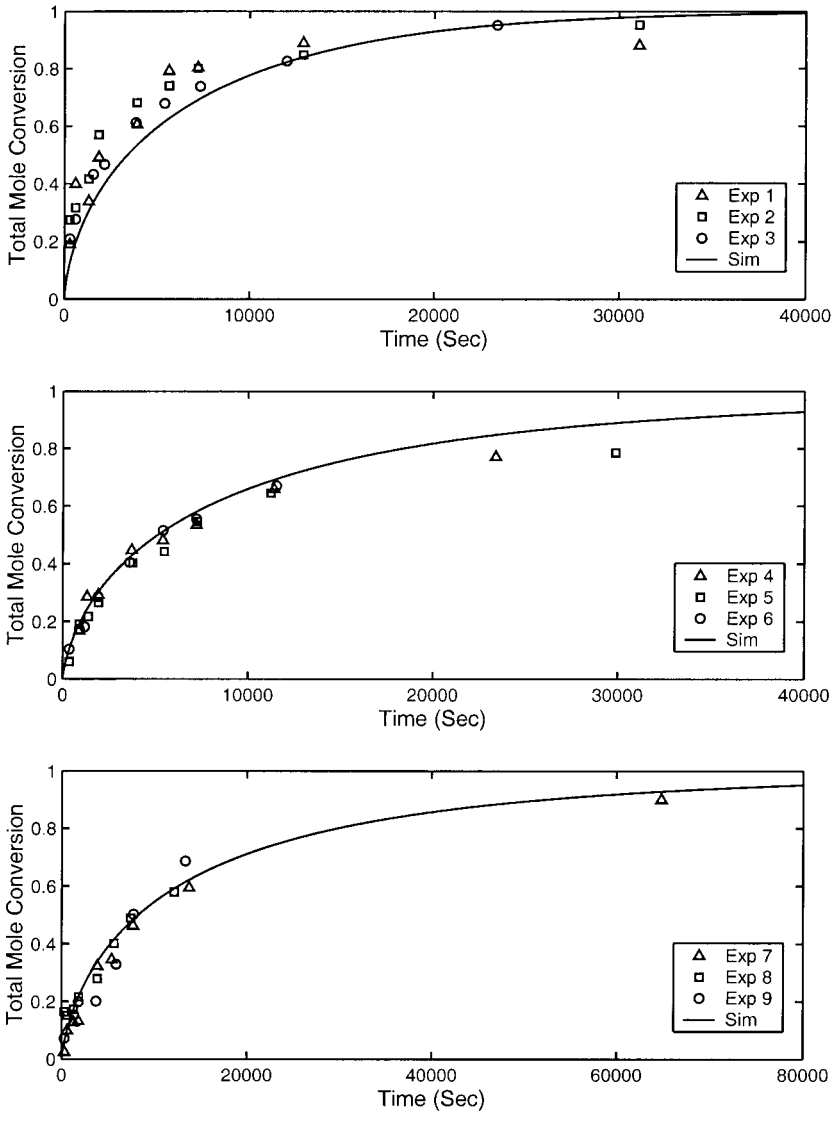

Figure 10 Model comparison to data of total monomer molar conversion versus time for atom transfer radical copolymerization of styrene and *n*-butyl acrylate at 110°C. Experimental data from Arehart et al.[41]

icals formed are quickly consumed by the capping reaction with TEMPO, so that other reactions, such as chain initiation and primary radical termination, are inhibited. The trapping reaction is so fast that almost every radical from thermal initiation is capped. Our findings show that for high TEMPO concentrations, the effective thermal initiation rate constant must be at least 10-fold greater than that in a conventional thermal styrene polymerization to match the induction period observed in experiments (Table V). However, after the TEMPO concentration drops to a low value, the conventional thermal initiation rate constant is appropriate again. In Appendix C, we show in detail that, in the presence of free TEMPO, many more radicals from thermal initiation will be able to initiate polymer chains than those in a conventional thermally initiated polymerization. For the cases of [St]/[TEMPO] = 50/1 and 100/1, the chains are short and the gel effect is not present. When the ratios of [St]/[TEMPO] are 200/1 and 400/1, the polymer chains become long at high conversion (Fig. 9), surpassing the chain entanglement threshold as suggested by De Gennes, and the gel effect becomes important. Figure 9 demonstrates the dependency of number-average chain length and polydispersity on monomer conversion, showing good agreement between the model and the limited data available.

Atom transfer radical copolymerization of styrene and *n*-butyl acrylate

Let us now validate our model with some examples from ATRP. Arehart et al.[41] conducted a detailed kinetic study of the atom transfer radical copolymerization of styrene and *n*-butyl acrylate using CuBr/4,4′-di(5-nonyl)-2,2′-bipyridine (dNbpy) as catalyst and methyl 2-bromopropionate (MBP) as the primary capped species. In this simulation, the kinetic param-

TABLE VI
Experimental Conditions in the ATRP of Styrene and *n*-Butyl Acrylate at 110°C Conducted by Arehart et al.[41]

Experiment	$f_{st,0}$	$[M]_0 : [MBP]_0 : [CuBr]_0 : [dNbpy]_0$
1	0.132	100 : 1.0 : 1.0 : 2.0
2	0.132	101 : 1.0 : 1.0 : 2.0
3	0.132	100 : 1.0 : 1.0 : 2.0
4	0.510	100 : 1.0 : 1.0 : 2.0
5	0.510	100 : 1.0 : 1.0 : 2.0
6	0.510	99 : 1.0 : 1.0 : 2.0
7	0.864	100 : 1.0 : 0.9 : 1.8
8	0.864	101 : 1.0 : 0.9 : 1.8
9	0.864	101 : 1.0 : 1.0 : 2.0

eters at 110°C can be found in Appendix B. The reversible capping reaction rate constants for styrene were reported earlier by Matyjaszewski et al.[42] The reversible capping reaction rate constants for *n*-butyl acrylate at 110°C are not explicitly reported in the literature; therefore, values are selected in this work in the range of reasonable values reported for various monomers using the same catalytic system. The reversible capping reaction rate constants for primary capped species are taken to be the same as those for dormant polymer chains ended with *n*-butyl acrylate.

Figure 10 shows multiple experimental conversion data sets measured by gas chromatography and simulation results for three different initial monomer ratios at 110°C. The detailed experimental conditions are

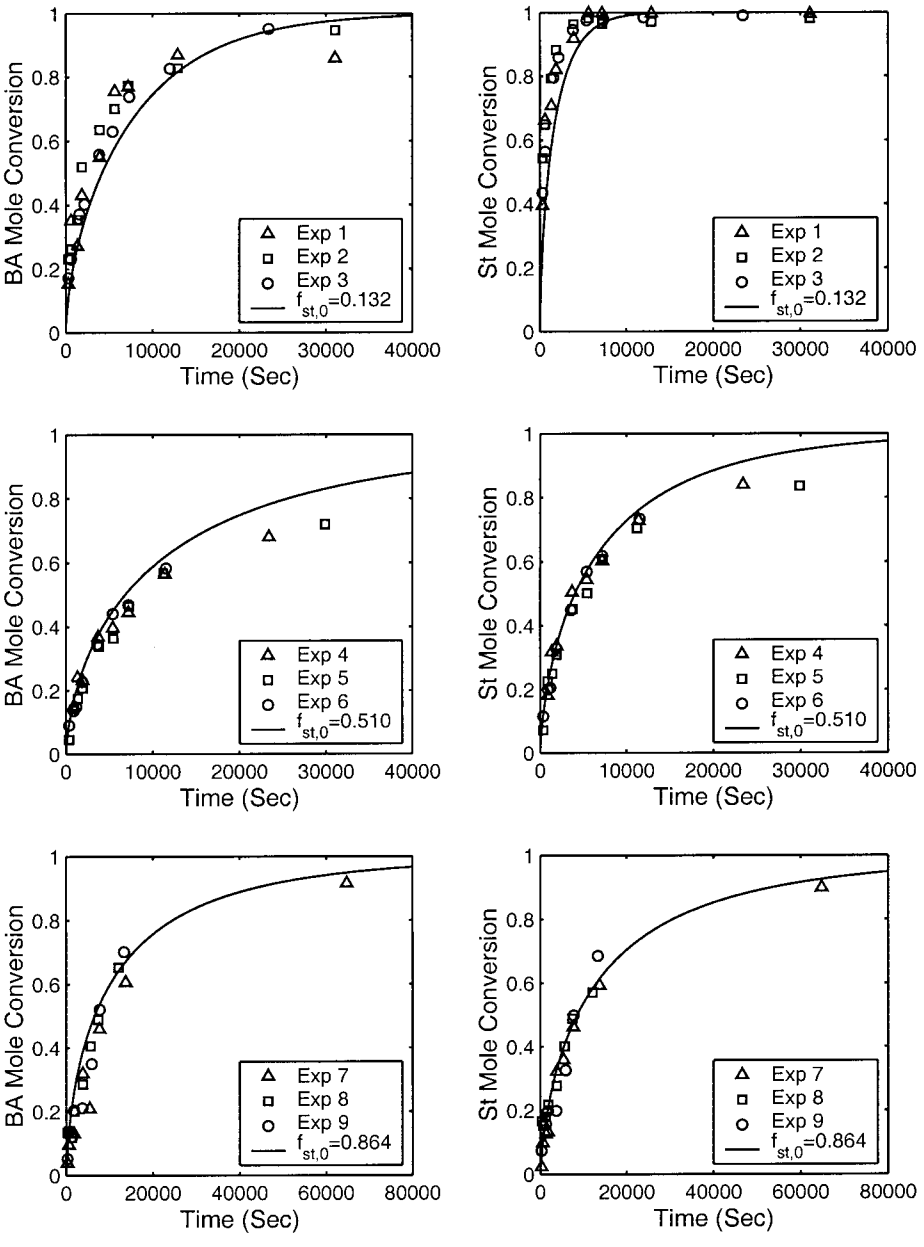

Figure 11 Model comparison to data of styrene and *n*-butyl acrylate molar conversions versus time for atom transfer radical copolymerization of styrene and *n*-butyl acrylate at 110°C. Experimental data from Arehart et al.[41]

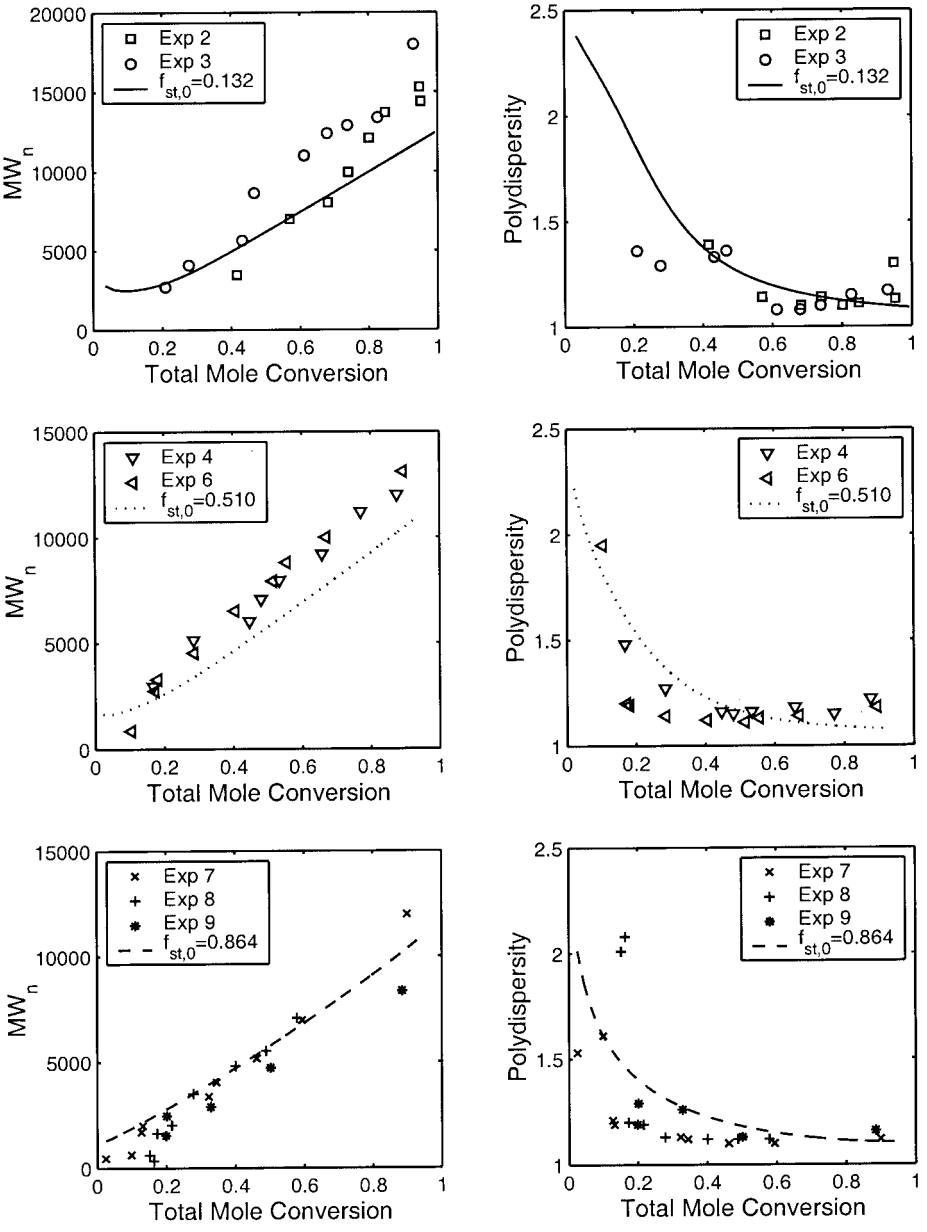

Figure 12 Model comparisons to data of number-average molecular weight versus total monomer molar conversion and to data of polydispersity versus total monomer molar conversion for atom transfer radical copolymerization of styrene and *n*-butyl acrylate at 110°C. Experimental data from Arehart et al.[41]

shown in Table VI. For each initial monomer ratio, three replicated experiments were conducted by Arehart et al.[41] to ensure reproducibility. The agreement of the model with experiments is good using the set of parameters shown in Appendix B.

Figure 11 shows comparisons of experimental data to simulations for the molar conversion of styrene and *n*-butyl acrylate versus time for three different initial monomer ratios. Note that monomer mixtures richer in styrene polymerize more slowly.

Figure 12 shows the development of number-average molecular weights and polydispersities with respect to total monomer molar conversion. The model underpredicts somewhat the number-average molecular weights, especially for $f_{st,0} = 0.132$ and $f_{st,0} = 0.510$ at high conversion. This underprediction may be attributed to unmodeled side reactions, which consume the primary capped species MBP in the experiment; thus, monomers incorporated into polymer chains are distributed over fewer chain seeds than the original amount of primary capped species, resulting a higher number-average chain molecular weight observed in the experiments than that in the model prediction. Note that the polymer has a very low polydispersity, regardless of initial monomer composition, and that the number-average chain length evolves linearly with respect to total monomer molar conversion.

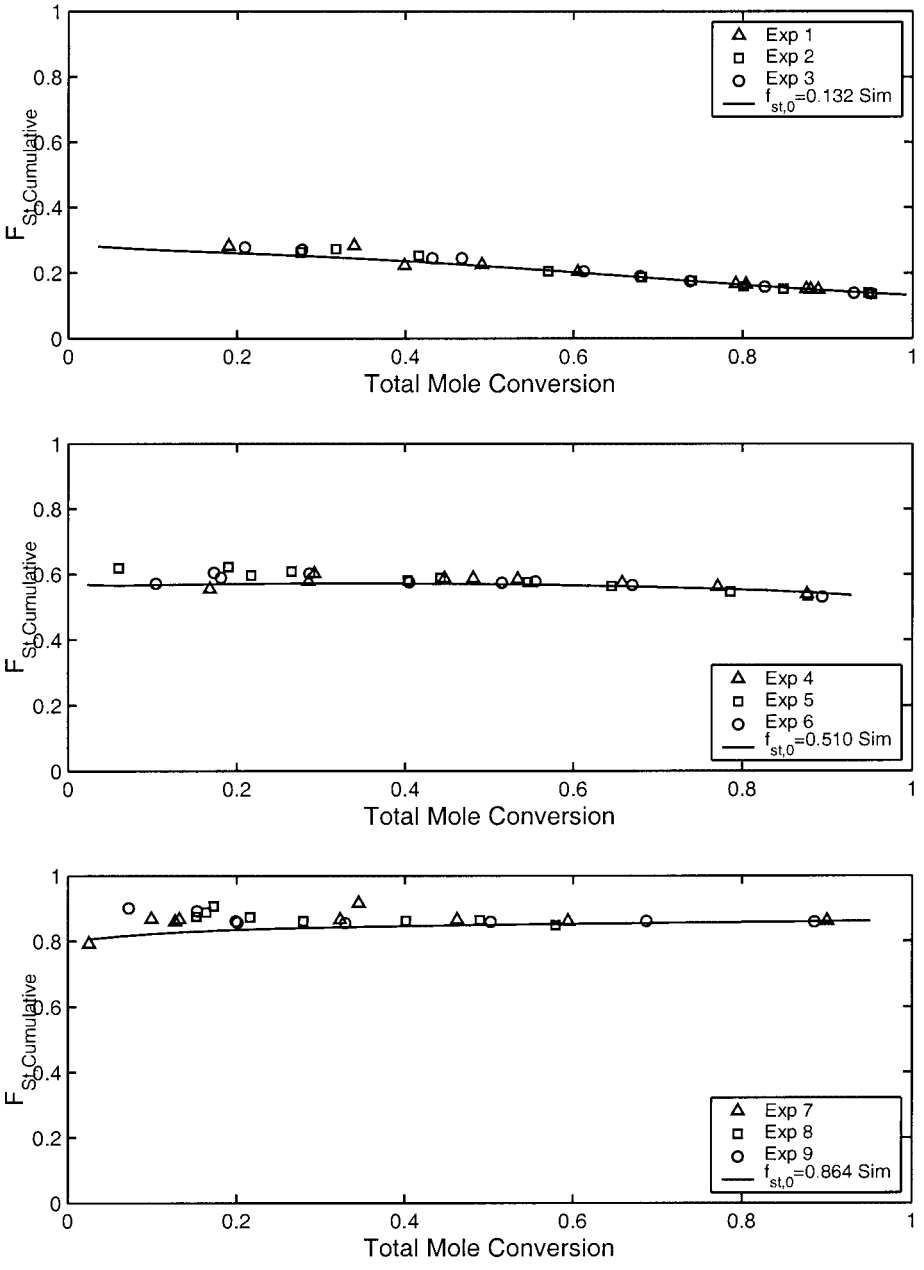

Figure 13 Model comparisons to data of styrene cumulative copolymer composition versus total monomer molar conversion for atom transfer radical copolymerization of styrene and *n*-butyl acrylate at 110°C. Experimental data from Arehart et al.[41]

In Figure 13, the cumulative copolymer composition (fraction of styrene) dependency on total monomer molar conversion predicted by the model is compared to the experimental data. The agreement is excellent, so the model can be considered predictive for for polymer composition using reported reactivity ratios (r_{st} = 0.79, r_{BA} = 0.26). This indicates that the living nature of the polymerization has a negligible effect on polymer composition.

In a conventional free-radical copolymerization, the copolymer composition may change with time, or "drift," from its initial value in a batch reactor. Thus dead polymer chains are formed instantaneously and new chains may show a very different composition than that of the previous ones. By contrast, in an ATRP, the instantaneous copolymer composition resulting from the monomer composition drift in the reactor is imprinted at every instant into the living polymer chains. Figure 14 shows the styrene instantaneous copolymer composition as a function of total monomer molar conversion. When $f_{st,0}$ = 0.132, the gradient in composition is quite significant along the polymer chain. However, when $f_{st,0}$ = 0.864, the composition is close to the azeotropic point, so that there is nearly uniform composition for the entire length. Thus the model allows one to design polymer products with a desired composition gradient along the chain.

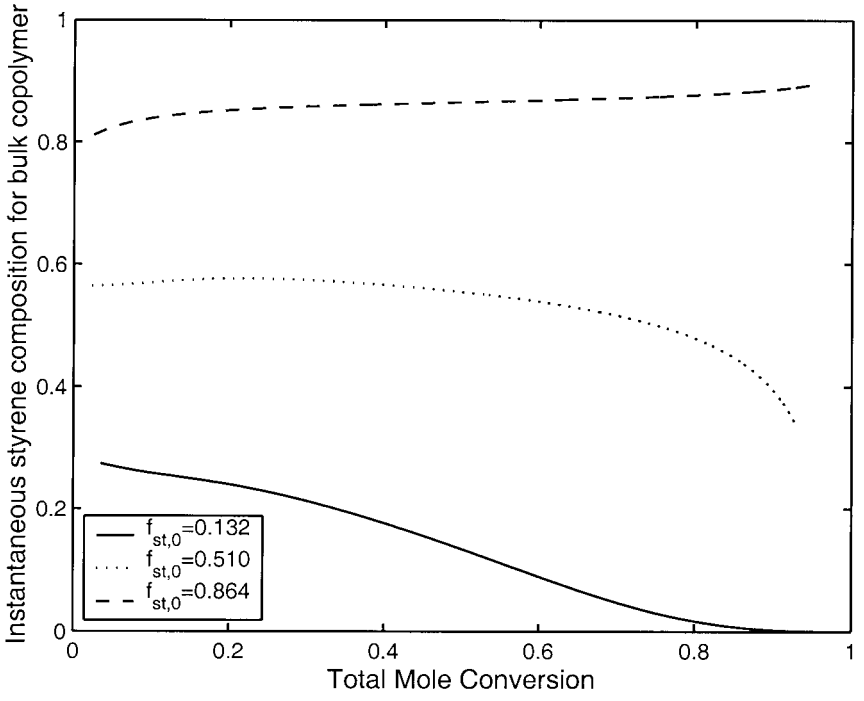

Figure 14 Simulation predictions for evolution of styrene instantaneous copolymerization with respect to total monomer molar conversion for atom transfer radical copolymerization of styrene and *n*-butyl acrylate at 110°C.

MODEL APPLICATIONS

Having demonstrated that our kinetic model is in good agreement with a variety of experimental data for both TEMPO-mediated and ATRP systems, we will apply the model to a number of important "living" free-radical process development issues.

Effects of capping rate constants and equilibrium constants

A good living free-radical polymerization process must have two important features: a reasonably fast polymerization rate and good control over polymer chain growth. Achieving this requires a good choice of chemical components, operating conditions, and reaction type. Screening for such a good living free-radical polymerization process is a major task, carried out by employing combinatorial chemistry at the moment. For instance, in the study of nitroxide-mediated styrene living free-radical polymerization, enhancing the polymerization rate is a very important issue. Hawker et al.[43] prepared a variety of initiating systems, which can be divided into two classes: unimolecular initiators (e.g., TEMPO-based derivatives) and bimolecular systems (e.g., a conventional initiator, such as BPO or AIBN used in conjunction with a TEMPO derivative). By manipulating the structure of TEMPO derivatives, kinetic parameters such as capping reaction rate constant and equilibrium constant can be changed. Hawker et al.[43] evaluated the influence of structural variations in TEMPO derivatives on polydispersity, molecular weight, conversion, and so forth. Among their results: unimolecular initiating systems impose better control over polymer chain growth than do bimolecular ones. In ATRP, Matyjazewski et al.[44] found that, by choosing different catalysts or ligands, the kinetic parameters such as the capping rate constant and/or equilibrium constant can be changed, greatly affecting control over polymer chain growth. As an aid to this type of screening, model predictions can be a guide to minimize the amount of experimentation necessary to discover a good living free-radical polymerization process.

In the following, we discuss the effects of the capping equilibrium constant, and the capping forward and backward rate constants as predicted by the model. The first system considered is a TEMPO-mediated styrene polymerization in which a unimolecular initiator (alkoxyamine) is used. The kinetic parameters are taken from Appendix B for TEMPO-mediated styrene polymerization, except that the capping rate constants and equilibrium constants may vary (as indicated in the figures). The simulation conditions are the same as used above to model the results of Tsujii et al.[40] Because TEMPO-mediated styrene polymerization normally runs at a high temperature, thermal initiation is important. To eliminate the potentially confounding effect of thermal initiation attributed to styrene monomer, we also discuss the ATRP of *n*-butyl acrylate, where the primary capped species is methyl 2-bromopropionate. $Cu^{I}Br$ with ligand is used as catalyst. The choice of ligand [e.g., 4,4′-di(5-nonyl)-2,2′-bipyridine (dNbpy), 2,2′-bipyridine (bpy), etc.] affects the values of k_{capf} and k_{capr}. In this study, repre-

TABLE VII
Simulation Conditions for the ATRP of *n*-Butyl Acrylate

$[BA]_0$	6.5 (mol/L)
$[\text{Primary Capped}]_0$	0.065 (mol/L)
$[Cu^IBr]_0$	0.065 (mol/L)
k_{capf}	5×10^9 L mol^{-1} s^{-1}
k_{capr}	0.05 L mol^{-1} s^{-1}
Temperature	90°C

sentative values of k_{capf} and k_{capr} are chosen, as shown in Table VII, but will be varied as noted when discussing the effect of capping equilibrium constants and capping rate constants. The details for simulation conditions can also be found in Table VII. For this second system, we also discuss how polymer properties and conversion may evolve when a certain amount of extra conventional initiator is introduced.

Figure 15 shows the effects of a change in the rate of the reversible capping reaction while the equilibrium constant was held fixed in TEMPO-mediated styrene polymerization at 125°C. Styrene thermal polymerization in the absence of alkoxyamine is also shown in Figure 15 as a reference. Figure 16 shows the effects of a change in the capping equilibrium constant in TEMPO-mediated styrene polymerization while the forward capping rate constant is unchanged. It is very interesting to find that in each of these cases, the growing radical concentration profiles almost coincide, the

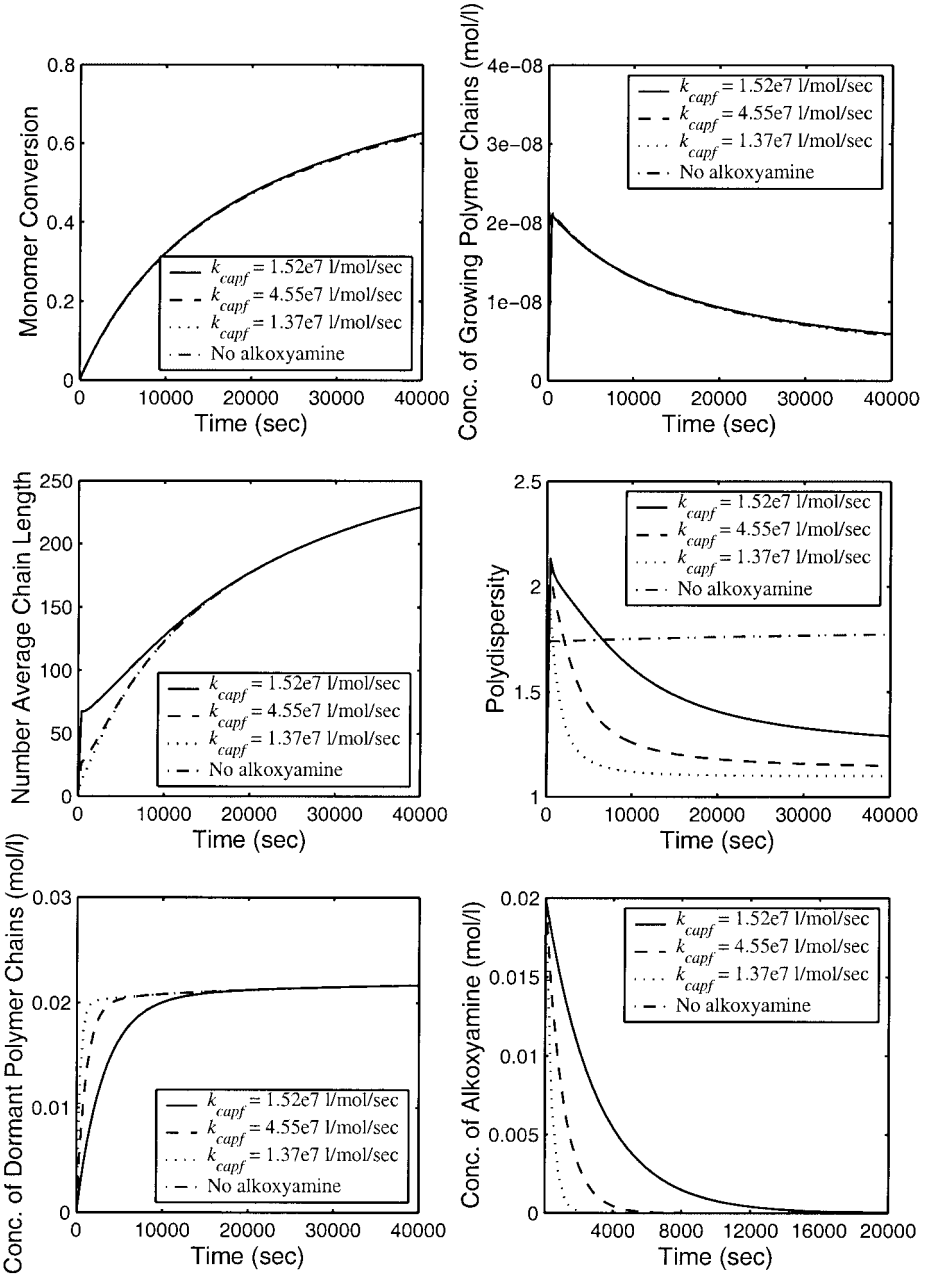

Figure 15 Effects of capping rate constant when the capping equilibrium constant remains unchanged ($k_{eq} = k_{capf}/k_{capr} = 1.59 \times 10^{12}$ L/mol for TEMPO-mediated styrene polymerization at 125°C.

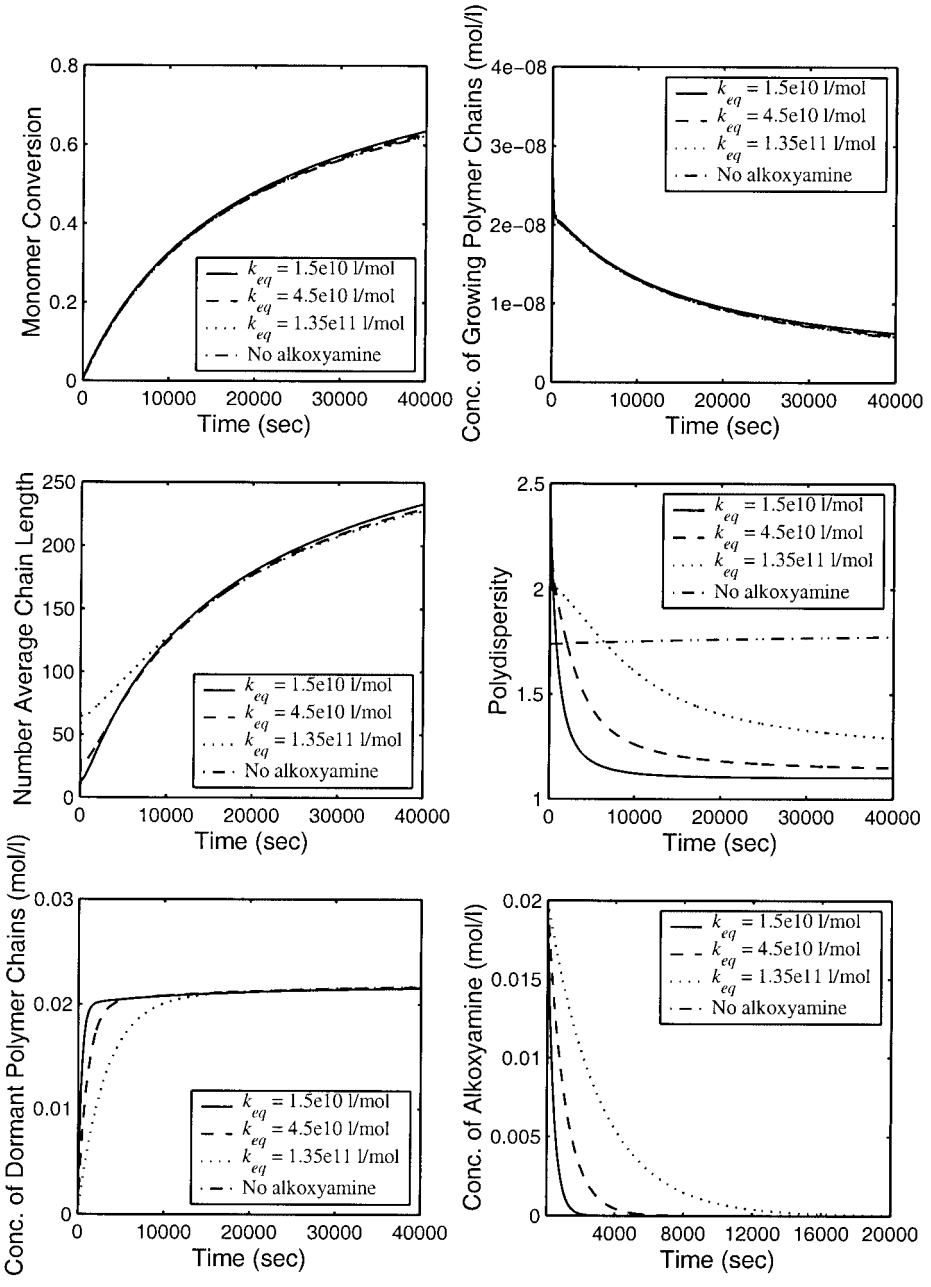

Figure 16 Effects of capping equilibrium constant when the forward capping rate constant remains unchanged ($k_{capf} = 1.61 \times 10^9$ L mol^{-1} s^{-1}) for TEMPO-mediated styrene polymerization at 125°C.

same as that in styrene thermal polymerization. Surprisingly, shifting the capping equilibrium constant has no effect on growing radical concentration development. Let us provide a physical explanation as to why the above observations occur. The reactions causing the birth and death of free radicals in this system involve thermal initiation of styrene, termination, and reversible capping reactions. A material balance for total free radicals gives the following:

$$\frac{d[R]}{dt} = R_i - k_t[R]^2 + k_{capr}[\text{TEMPO} - R] - k_{capf}[R][\text{TEMPO}] \quad (9)$$

where $[R]$ is the concentration of total free radicals, R_i is the generation rate of free radicals attributed to thermal initiation, $[\text{TEMPO} - R]$ is the total concentration of dormant polymer chains and alkoxyamine. Note that the values of $k_{capf}[R][\text{TEMPO}]$ and $k_{capr}[\text{TEMPO} - R]$ must be much larger than those of R_i and $k_t[R]^2$ to have a "living" polymerization. In the case of a monomer that cannot polymerize through thermal initiation, the value of R_i is zero and the concentration of total free radicals in the system is solely determined by the equilibrium constant $k_{eq} = k_{capf}/k_{capr}$, with only a tiny contribution from the termination step. However, if R_i is indeed significant,

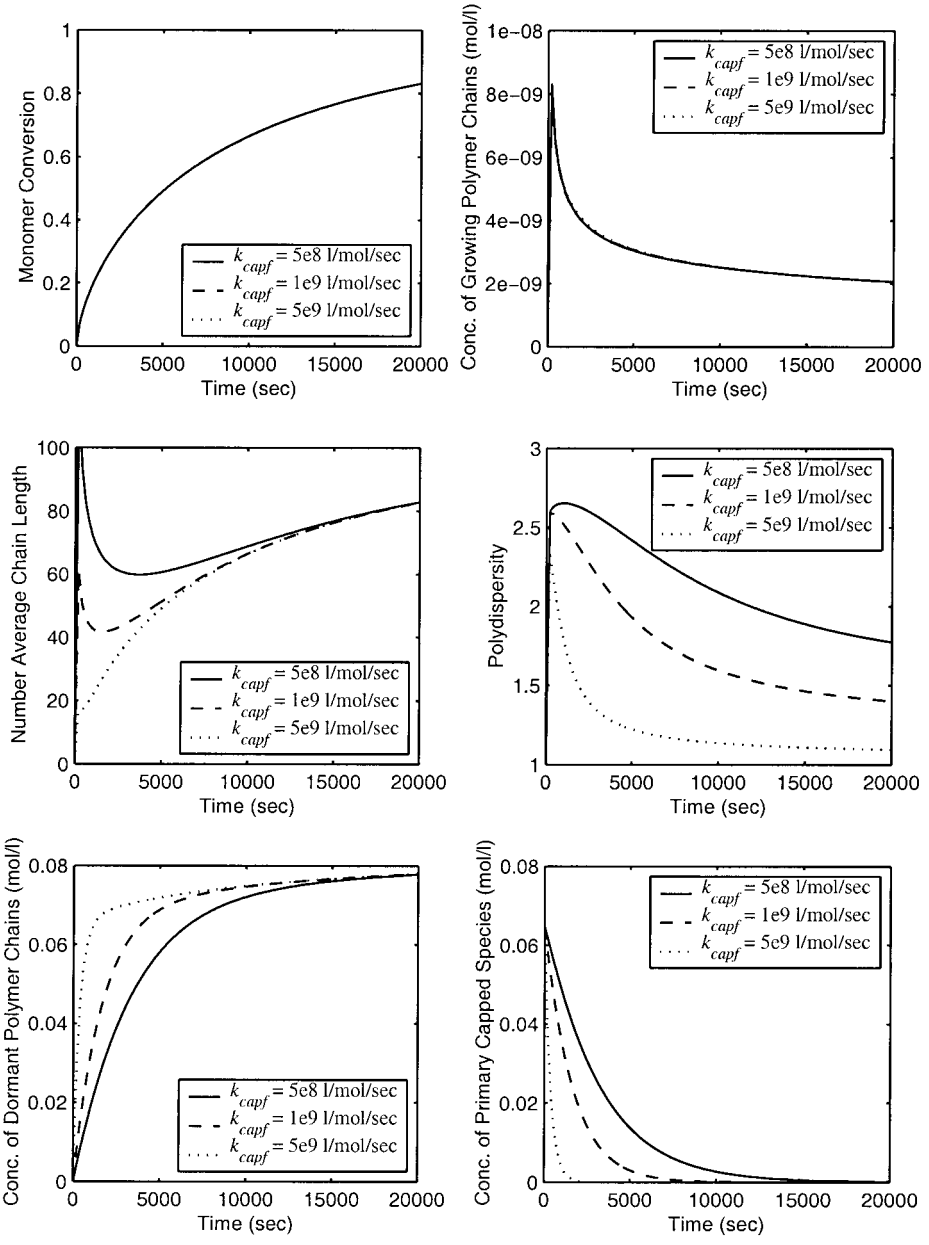

Figure 17 Effects of capping rate constant when the capping equilibrium constant remains unchanged ($k_{eq} = k_{capf}/k_{capr} = 1 \times 10^{11}$) for ATRP of *n*-butyl acrylate at 90°C.

the radicals generated initially because of thermal initiation are rapidly capped by free TEMPO, resulting in a decrease of free TEMPO in the system and a shift in the reversible capping reaction in favor of forming dormant species. The reversible capping reaction rapidly achieves a quasi-steady state, so that those terms in eq. (9) cancel. In this case, it is the balance of thermal initiation and termination rather than the reversible capping reaction that determines the concentration level of growing radicals. Because the styrene concentrations are the same in both cases, the same growing radical concentration profiles are expected. However, it is seen that only for rapid radical release of growing radicals from alkoxyamine and dormant polymer chains is a low polydispersity achieved. Shifting the capping equilibrium constant by changing the forward capping rate constant has a negligible effect on polymer chain growth (e.g., number-average chain length and polydispersity).

Let us now consider the case of ATRP of *n*-butyl acrylate at 90°C. Figure 17 shows the effects of changing the capping rate constants but maintaining the capping equilibrium constant unchanged, whereas Figures 18 and 19 show the effects of a change in the capping equilibrium constant while in Figure 18 the backward capping rate constant is unchanged and in Figure 19 the forward capping rate constant is unchanged. Note in this study, no extra conventional initiator has been used. The concentration of growing radicals is determined completely by the reversible

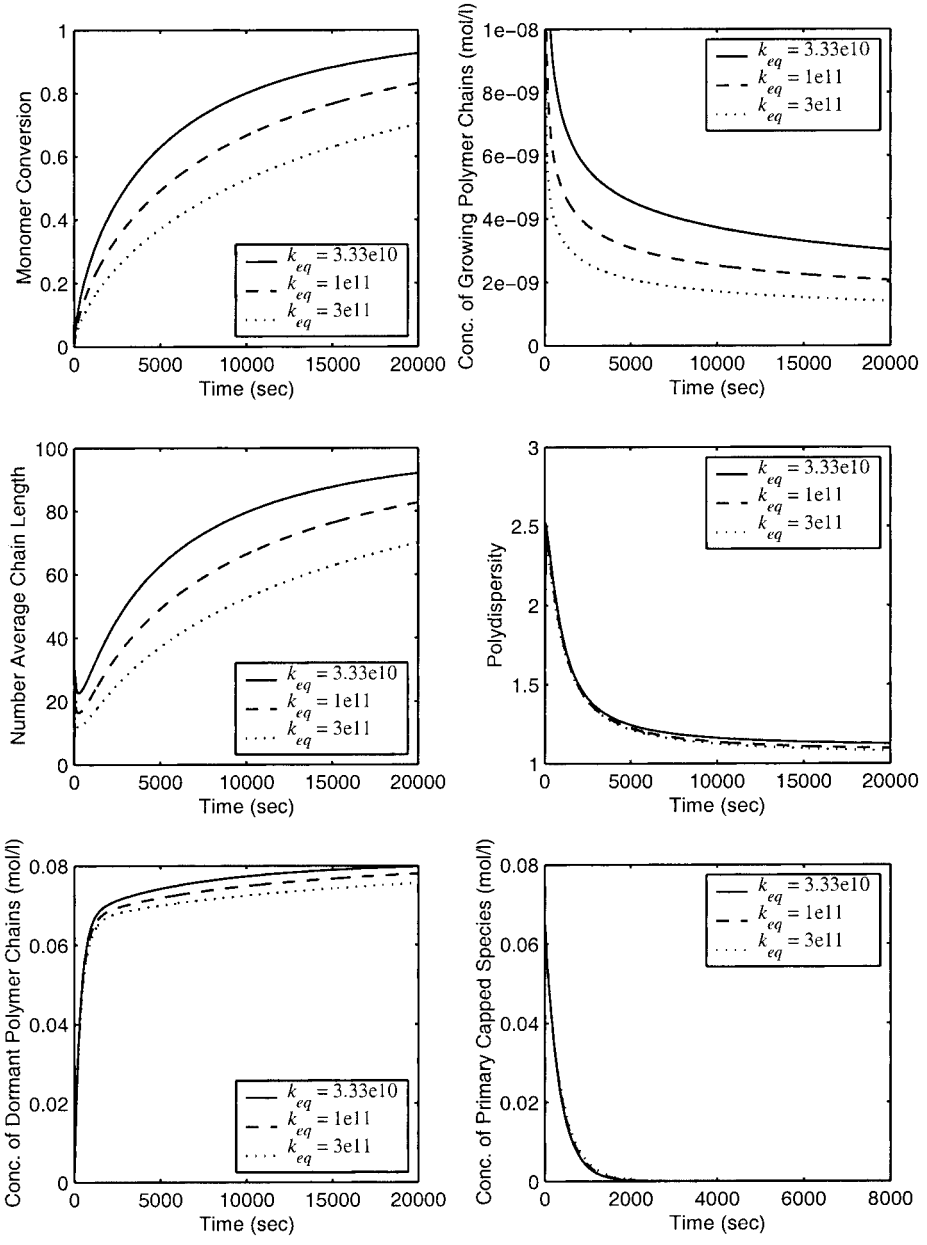

Figure 18 Effects of capping equilibrium constant when the backward capping rate constant remains unchanged (k_{capr} = 0.05 L mol^{-1} s^{-1}) for ATRP for *n*-butyl acrylate 90°C.

capping reactions (i.e., the capping equilibrium constant). As shown in Figure 17, the growing radical concentration profiles are the same when the capping equilibrium constants are the same, even though the individual capping rate constant has been changed; therefore the conversion profiles coincide. In Figures 18 and 19, increasing the capping equilibrium constant causes a shift of the reversible reaction between growing and dormant polymer chains in favor of dormant polymer chains; therefore, a lower concentration of growing polymer chains is observed, which results in a slower polymerization rate. In Figures 17 and 19, an increased backward capping rate constant results in polymers with a lower polydispersity because the primary capped species and dormant polymer have a better chance at growth before there is any significant degree of conversion.

As we saw above for TEMPO-mediated styrene polymerization where thermal initiation is significant at high temperature, the balance of thermal initiation and termination determines the concentration level of growing radicals. Thus one expects something similar if one introduces extra conventional initiator in ATRP of *n*-butyl acrylate. In this case, the reactions that result in the birth and death of radicals involve initiation from the conventional initiator, termination, and reversible capping reactions. If the rate of initiation is quite significant, the capping reactions will quickly reach a quasi-steady state and the balance of initiation attributed to the decomposition of initiator and termi-

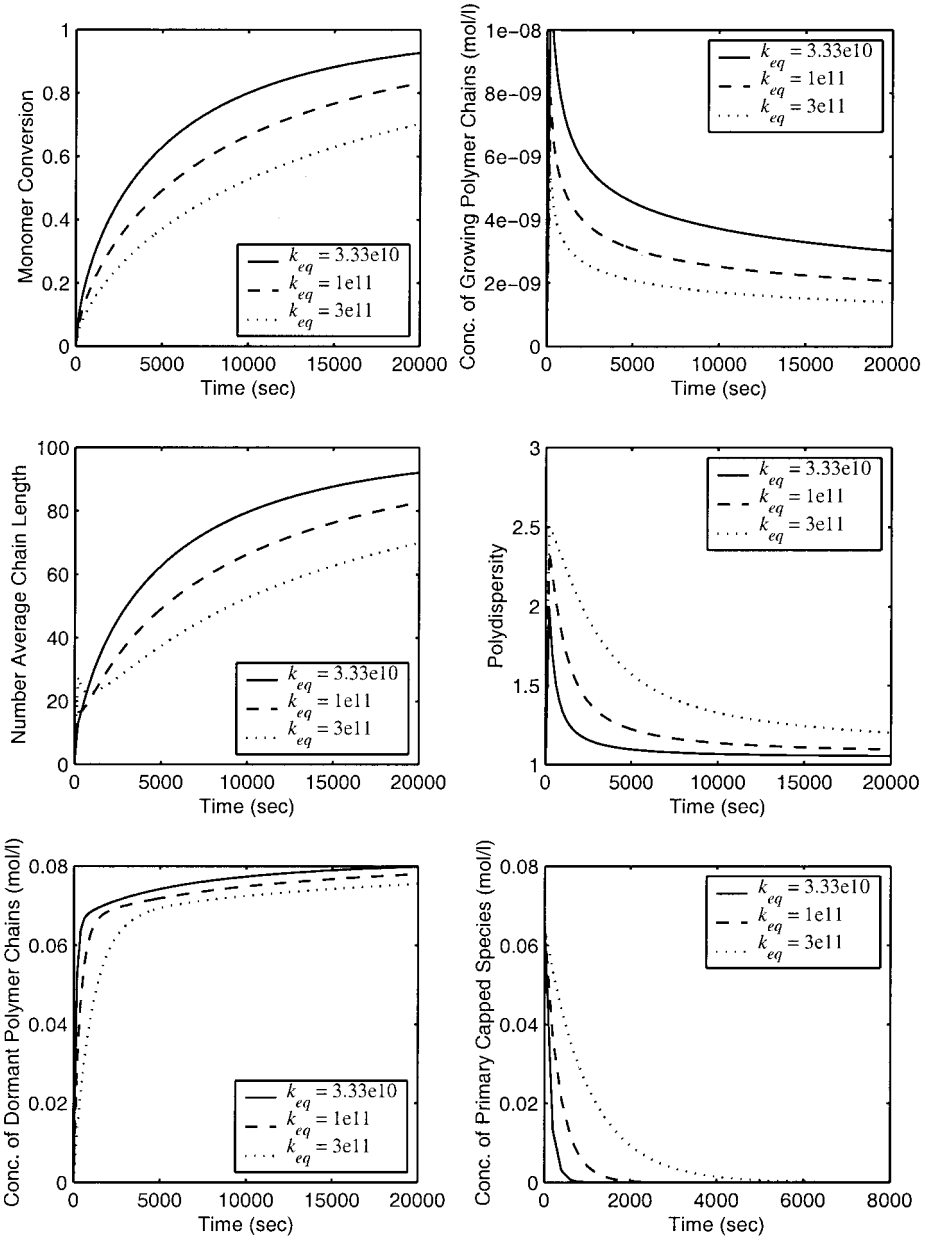

Figure 19 Effects of capping equilibrium constant when the forward capping rate constant remains unchanged ($k_{capf} = 5 \times 10^9$ L mol^{-1} s^{-1}) for ATRP of *n*-butyl acrylate at 90°C.

nation will determine the concentration level of growing radicals in the system. Obviously, faster polymerization could be achieved with added initiator, but the generation rate of dead polymer is also higher because of a higher concentration of free radicals.

Let us illustrate these points through two examples. In the first example, conventional initiator AIBN is used in the ATRP of *n*-butyl acrylate. The initial concentration of AIBN is fixed at 0.0002 mol/L, which ensures that chemical initiation is significant. Polymerization of *n*-butyl acrylate using only AIBN is also presented as a reference. Figure 20 shows the effects of changing the capping rate constants but maintaining the capping equilibrium constant unchanged. Note that the concentration of growing radicals is much higher and batch time much shorter by adding extra conventional initiator (Fig. 17 and 20). If we vary the equilibrium constant up and down by a factor of 3, while keeping the backward capping rate constant unchanged, the model predicts no significant effect on conversion and polymer properties. On the other hand, if we vary the equilibrium constant while keeping the forward capping rate constant, we have results identical to Figure 20. Thus it is the backward rate constant that is controlling under these conditions and the equilibrium constant is not important. This shows again that the rapid exchange of primary capped species and dormant polymer is essential to low polydispersity.

Model simulations suggest that using primary capped species in conjunction with some amount con-

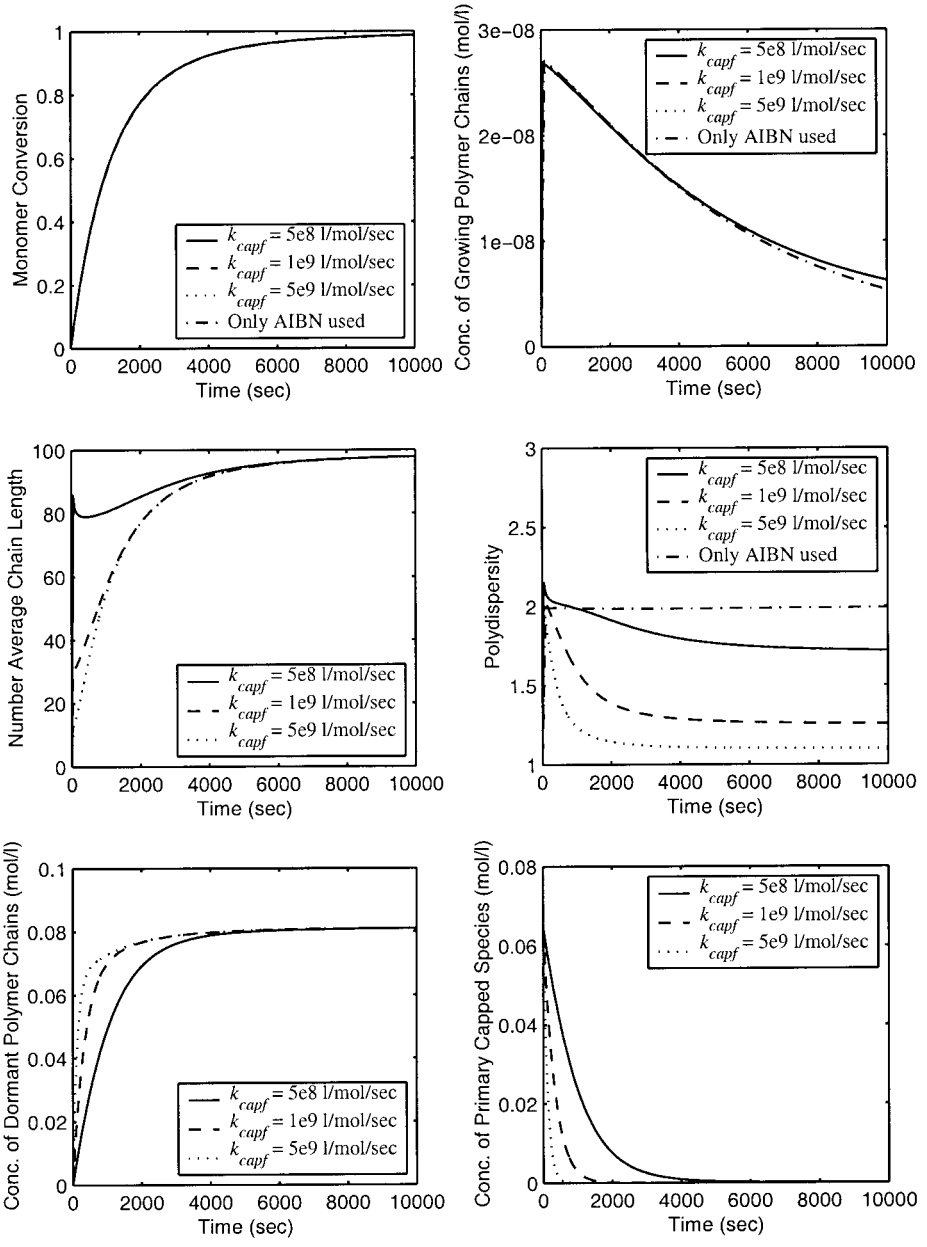

Figure 20 Effects of capping rate constant when the capping equilibrium constant remains unchanged ($k_{eq} = k_{capf}/k_{capr} = 1 \times 10^{11}$) for ATRP of *n*-butyl acrylate at 90°C. Extra initiator, AIBN, is used. $[AIBN]_0 = 0.0002$ mol/L.

ventional initiator may achieve both an enhanced polymerization rate and better control over chain architecture. However, there is the question of how much additional initiator is optimal. Figure 21 shows the influence of three levels of initiator addition to the batch charge when $k_{capf} = 5 \times 10^9$ mol/L^{-1}/s^{-1} and $k_{eq} = 1 \times 10^{11}$. The three levels of initiator addition all guarantee that the generation of radicals due to initiation is significant. Notice that initially the growing radical concentration is much higher, although the termination reaction eventually drives this down to a value close to that with no additional initiator. The increased radicals have only a small effect on the conversion of primary capped species to dormant polymers because this requires the decomposition of primary capped species. The increase in growing radical concentration greatly increases the polymerization rate and the rate of chain extension; however, significant conversion occurs before most of the primary capped species are converted to dormant polymer. Thus true living polymerization is not achieved until about 50% monomer conversion, resulting in higher ultimate polydispersities than those in the case without added initiator. It is this, and not the additional dead polymer, that causes the polydispersity increase. Therefore, the charge of additional initiator must be carefully chosen to enhance polymerization while still maintaining good control over polymer chain growth. Our model provides a means to guide this choice.

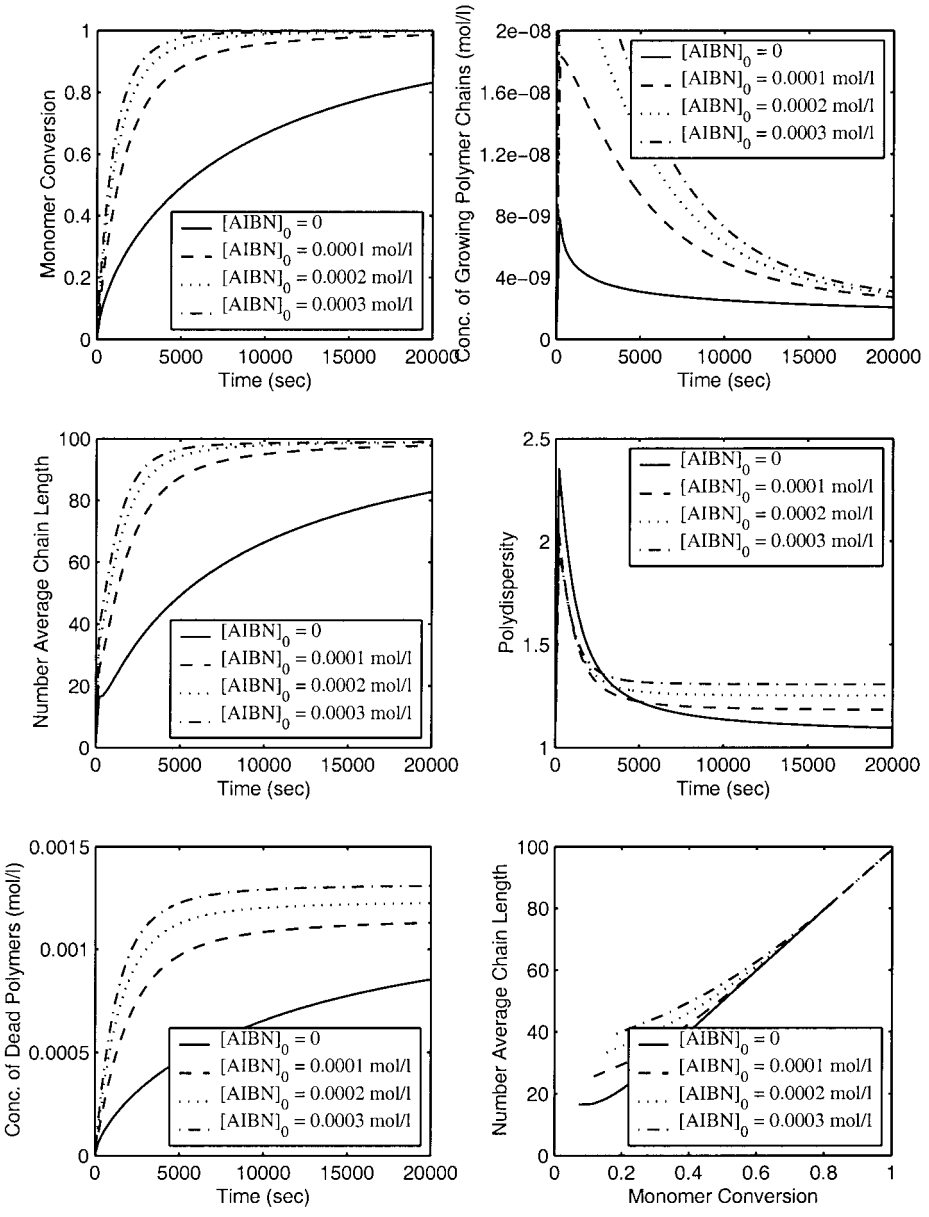

Figure 21 Effects of adding different amount of extra initiator for ATRP of *n*-butyl acrylate at 90°C.

Preparation of gradient copolymers in a semibatch reactor

The advantages of "living" free-radical polymerization are not just limited to the ability to produce homopolymers with narrow molecular weight distributions. Another important advantage is the capability of preparing copolymers with tailored structures. We thus set out to show how the model benefits the development of new products in "living" free-radical polymerization. Matyjaszewski et al. reported a wide variety of copolymerization systems using ATRP, such as styrene/*n*-butyl acrylate,[41,45] styrene/acrynolitrile,[46] and methyl methacrylate/*n*-butyl acrylate.[23] They pointed out that two types of gradient polymers can be synthesized, depending on the reactivity ratios of the two comonomers. If the reactivity ratios of the two monomers show a big difference, then in a batch reactor, one monomer is preferentially incorporated into polymer chains and spontaneous gradients solely determined by the reactivity ratios are introduced into polymer chains. Controlled gradients also can be introduced into polymer chains through the use of a semibatch reactor, varying the feed rate of one monomer, and thus forcing the change of monomer ratio in the reactor. Note that Matyjaszewski et al.[45,46] presented experimental results in a semibatch reactor for styrene/*n*-butyl acrylate and styrene/acrylonitrile copolymerization through ATRP, where they prepared copolymers with controlled gradients in copolymer composition. To show that there is more flexibility for controlling copolymer composition gradients in a semibatch reactor and the model provides a guide for

TABLE VIII
Operating Conditions in Preparation of Gradient Copolymers

Case	Feed rate	Feed composition	Initial charge
(A)	0.04 cm^3/s	$[BA]_f$ = 6.34 mol/L	$[St]_0$ = 8.14 mol/L
(B)	0.01 cm^3/s	$[St]_f$ = 6.77 mol/L	$[MBP]_0$ = 0.0814 mol/L
		$[BA]_f$ = 1.07 mol/L	$[St]_0$ = 6.77 mol/L
			$[BA]_0$ = 1.07 mol/L
			Volume = 300 cm^3

this, we present a case study for the atom transfer radical copolymerization of styrene and *n*-butyl acrylate in a semibatch reactor.

Two different operations for the preparation of copolymers with different gradients along the polymer chain are simulated. The details of the operating conditions are shown in Table VIII. As shown in Figures 22 and 23, two different gradients in copolymer composition were created in the polymer chains. For Case A, both the styrene content and sequence length decrease with chain length; at the same time the final polydispersity is low. For the second operation shown in Figure 23, the reactor quickly reaches a "steady state," corresponding to starved feed operation for both styrene and *n*-butyl acrylate concentration and then produces a constant composition copolymer with steadily increasing chain length and decreasing polydispersity. Through this semibatch operation one obtains the narrow MWD of the batch reactor and the uniform composition and chain sequence of the CSTR.

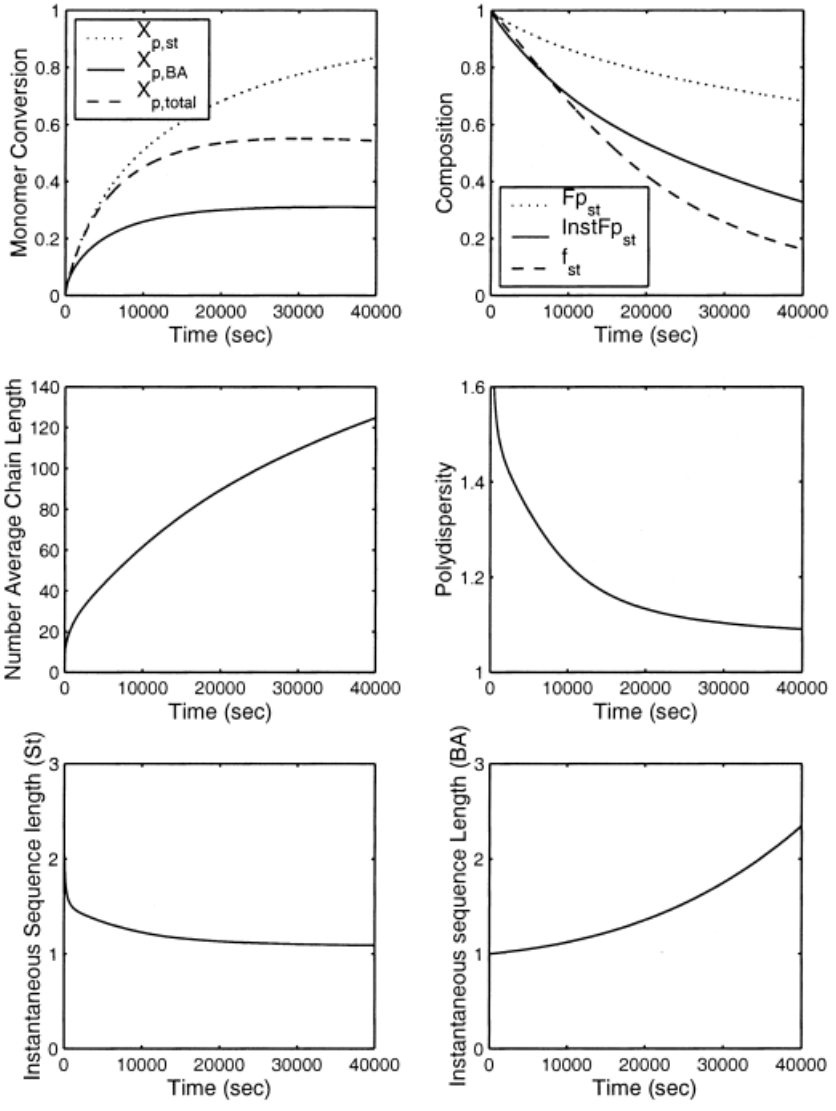

Figure 22 Semibatch copolymerization of styrene and *n*-butyl acrylate at 110°C in a semibatch reactor: Case A.

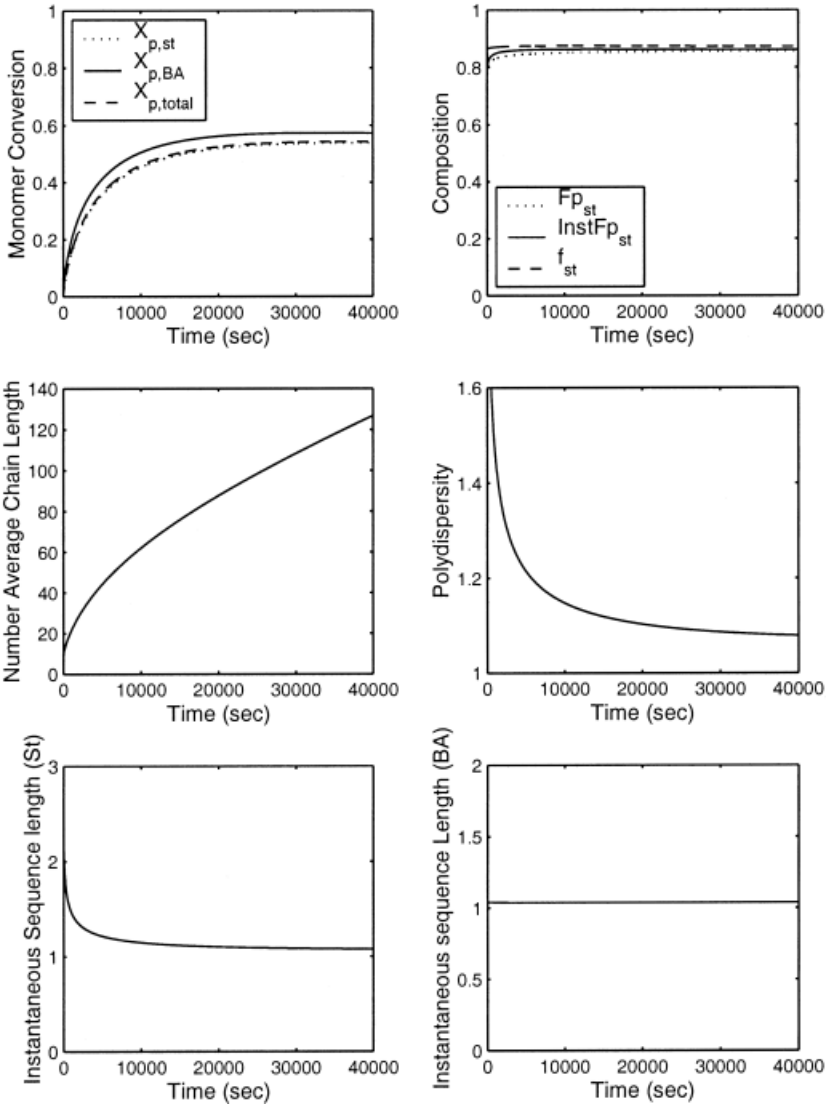

Figure 23 Semibatch copolymerization of styrene and *n*-butyl acrylate at 110°C in a semibatch reactor: Case B.

Effect of residence time distribution

Many experimental studies for "living" free-radical polymerization have been carried out in a batch reactor. A batch reactor is unique because all reactants have the same residence time in the reactor. Therefore, the residence time distribution effect is eliminated in batch experimental studies. However, in practice a continuous process may be more suitable for the preparation of polymers that require larger volume production and uniform quality. In this case, continuous stirred tank or tubular reactors may be employed. However, reactant materials, entering these reactors, may experience different residence times before exiting the reactors. Thus, it is important to know how the reactor residence time distribution may interact with "living" free-radical polymerization chemistry and whether "living" free-radical polymerization can be achieved.

Atom transfer radical copolymerization of styrene and *n*-butyl acrylate is used as a model system. To construct different residence time distributions, a series of CSTRs consisting of 4, 8, and 16 tanks are considered. Each reactor has a volume of 1000 cm^3. The feed rates shown in Table IX are chosen to ensure that the total residence time is the same in each case. The polymerization is catalyzed by CuBr/(dNbpy) at 110°C. MBP is used as the primary capped species. The kinetic parameters for *n*-butyl acrylate and styrene are the same as in the previous batch case. Feed compositions are as follows: styrene 3.98 mol/L, *n*-butyl acrylate 3.24 mol/L and MBP 0.065 mol/L.

The model results in Figure 24 show that as the number of CSTRs increases, the residence time distri-

TABLE IX
Feed Rates for Three Series of CSTRs

Total number of tanks	Feed rate (cm^3/s)
4	0.05
8	0.1
16	0.2

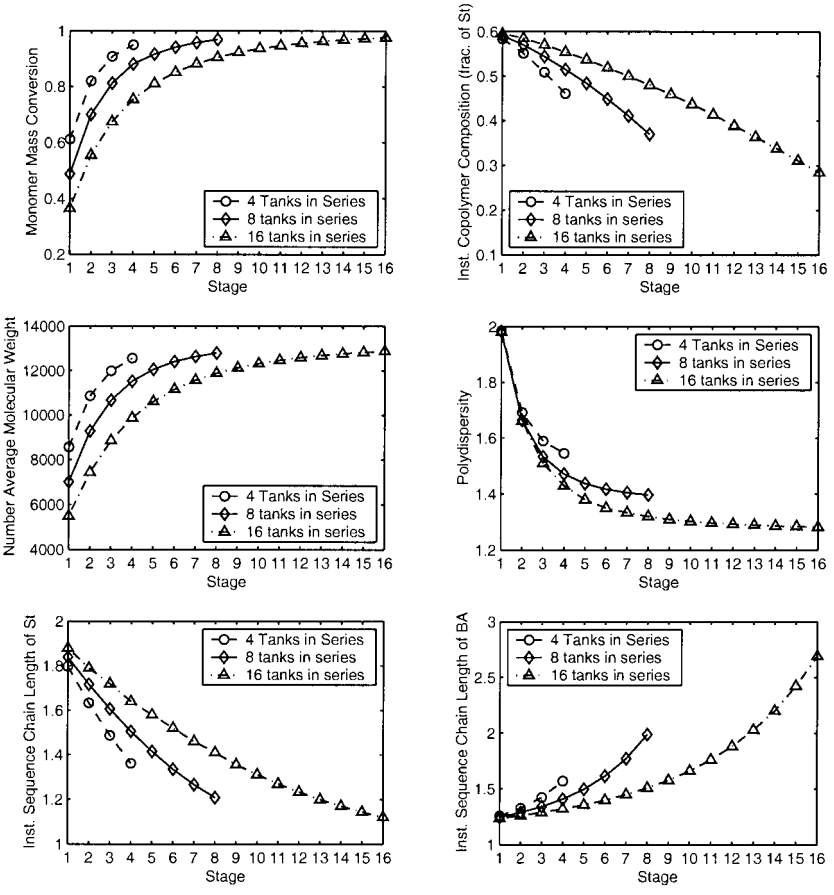

Figure 24 Development of monomer conversion and polymer properties in series of CSTRs.

bution is narrower; therefore, a slightly higher conversion at the outlet of the last tank is achieved with 16 tanks. Although the final number-average molecular weight is essentially the same for each case, the polymer polydispersity is strongly affected by the residence time distribution. Even with 16 tanks, the residence time distribution is still somewhat broader than that of the batch or semibatch reactor, so that the polydispersity is limited to about 1.3. It is expected that a well-designed tubular reactor could have a much narrower residence time distribution and thus lower polydispersity.

The series of stirred tanks also produces a tapered polymer chain because the monomer composition varies at each stage, as it would in a batch reactor. As the residence time distribution becomes narrower, the gradient in composition is much steeper. One advantage of a series of CSTRs is that these composition gradients could be remedied by by feeding additional amounts of the more reactive monomer into each tank to keep the monomer composition constant along the train.

In summary, the residence time distribution has a significant effect on the polymer properties for "living" free-radical polymerization. Even though a very large number of in-series CSTRs is employed, the residence time distribution limits polydispersity.

CONCLUSIONS

A comprehensive model for "living" free-radical copolymerization, describing both atom transfer radical polymerization and nitroxide-mediated polymerization, has been developed in this study. The model has been validated against experimental data for nitroxide-mediated styrene polymerization and atom transfer radical copolymerization of styrene and *n*-butyl acrylate. Simulations demonstrate how this model can be employed for improved process development and operation. Model predictions show that operating a "living" free-radical process at a reasonably fast polymerization rate can be achieved by using primary capped species in conjunction with a conventional initiator. Choosing agents to have an appropriate capping equilibrium constant and capping reaction rate constants is also important. These and other factors have been illustrated through this fundamental model. The model has been used to analyze the operation of semibatch reactors to produce controlled polymer architectures, and the effects of residence time distributions in continuous tank reactors have also been studied. More results and additional details are available in Zhang.[37]

The authors are grateful to the industrial sponsors of the University of Wisconsin Polymerization Reaction Engineer-

ing Laboratory (UWPREL) and to the National Science Foundation for financial support.

APPENDIX A: KINETIC MODEL

This appendix shows the details of kinetic model equations for "living" free-radical polymerization shown in Table I.

Rate of change of nonpolymer species

Here the rates of change of all nonpolymer species are shown in detail.

- Solvent

$$\mathrm{R}_{C_S} = -\mathrm{C}_\mathrm{S} \sum_{j=1}^{N_{mon}} k_{ctSj}\mu_{0,j} \tag{10}$$

- Chain-transfer agent (CTA)

$$\mathrm{R}_{C_{CTA}} = -\mathbf{C}_{CTA} \sum_{j=1}^{N_{mon}} k_{ctCTAj}\mu_{0,j} \tag{11}$$

- Inhibitor

$$\mathrm{R}_{C_X} = -\mathrm{C}_\mathrm{X} \sum_{j=1}^{N_{mon}} k_{tXj}\mu_{0,j} - k_{tX0}C_X C_{P_0} \tag{12}$$

- Initiator

$$R_{C_I} = -k_{inid}C_I \tag{13}$$

- Primary capped species

$$\mathrm{R}_{C_{\mathrm{PriCapped}}} = k_{\mathrm{CapPri}\mathbf{F}}C_{P_0}C_{CAP} - k_{\mathrm{CapPri}\mathbf{R}}C_{\mathrm{PriCapped}}C_{CAT} \tag{14}$$

- Catalyst

$$R_{C_{CAT}} = k_{\mathrm{CapPri}\mathbf{R}}C_{P_0}C_{CAP} - k_{\mathrm{CapPri}\mathbf{R}}C_{\mathrm{PriCapped}}C_{CAT} + C_{CAP}\sum_{j=1}^{N_{mon}} k_{\mathrm{cap}Fj}\mu_{0,j} - C_{CAT}\sum_{j=1}^{N_{mon}} k_{\mathrm{cap}Rj}\nu_{0,j} \tag{15}$$

- Capping agent

$$R_{C_{CAP}} = k_{\mathrm{CapPri}\mathbf{R}}C_{\mathrm{PriCapped}}C_{CAT} - k_{\mathrm{CapPri}\mathbf{F}}C_{P_0}C_{CAP} + C_{CAT}\sum_{j=1}^{N_{mon}} k_{\mathrm{cap}Rj}\nu_{0,j} - C_{CAP}\sum_{j=1}^{N_{mon}} k_{\mathrm{cap}Fj}\mu_{0,j} \tag{16}$$

- Monomer i

$$R_{C_{Mi}} = -k_{pi}C_{P_0}C_{Mi} - x(i)k_{spini}C_{Mi}^{y(i)} + \sum_{j=1}^{N_{mon}} k_{pij}\mu_{0,j}C_{Mi} - \sum_{j=1}^{N_{mon}} k_{ctMij}\mu_{0,j}C_{Mi} \tag{17}$$

- Primary radical

$$\begin{aligned} R_{C_{\mathbf{P}0}} = {} & 2fk_{inid}C_I + k_{\mathrm{CapPri}R}C_{\mathrm{PriCapped}}C_{CAT} \\ & - k_{\mathrm{CapPri}\mathbf{F}}C_{P_0}C_{CAP} - \sum_{i=1}^{N_{mon}} k_{pi}C_{P_0}C_{Mi} \\ & + C_S\sum_{j=1}^{N_{mon}} k_{ctSj}\mu_{0,j} + C_{CTA}\sum_{j=1}^{N_{mon}} k_{ctCTAj}\mu_{0,j} \\ & + \sum_{j=1}^{N_{mon}} k_{ctSpj}\mu_{0,j} - k_{tX0}C_X C_{P_0} \\ & - (k_{tcpri} + k_{tdpri})C_{P_0}\left(\sum_{j=1}^{N_{mon}} \mu_{0,j} + C_{P_0}\right) \end{aligned} \tag{18}$$

Rate of change of polymer species

- Growing polymer chains with end group j

$$\begin{aligned} R_{P_{\mathbf{n},j}} = {} & \delta(\mathbf{n} - \boldsymbol{\delta}_\mathbf{j})\left(k_{pj}C_{P_0}C_{Mj} + \sum_{i=1}^{N_{mon}} k_{ctMji}\mu_{0,i}C_{Mj} + x(j)k_{spinij}C_{Mj}^{y(j)}\right) + \sum_{i=1}^{N_{mon}} k_{pji}C_{Mj}P_{\mathbf{n}-\boldsymbol{\delta}_\mathbf{j},i} \\ & - \sum_{i=1}^{N_{mon}} k_{pij}C_{Mi}P_{\mathbf{n},j} - \alpha_j P_{\mathbf{n},j} \\ & - k_{\mathrm{Cap}Fj}P_{\mathbf{n},j}C_{CAP} \\ & + k_{\mathrm{Cap}Rj}Q_{\mathbf{n},j}C_{CAT} - \sum_{i=1}^{N_{mon}}\sum_{\mathbf{m}=\mathbf{0}}^{\infty} k_{cdij}P_{\mathbf{n},j}Q_{\mathbf{m},i} \\ & + \sum_{i=1}^{N_{mon}}\sum_{\mathbf{m}=\mathbf{0}}^{\infty} k_{cdji}P_{\mathbf{m},i}Q_{\mathbf{n},j} \end{aligned} \tag{19}$$

where

$$\begin{aligned} \alpha_j = {} & k_{ctSj}C_\mathbf{S} + k_{ctSpj} + k_{ctCTAj}C_{CTA} \\ & + \sum_{i=1}^{N_{mon}} k_{ctMij}C_{Mi} + k_{tXj}C_X \\ & + \sum_{i=1}^{N_{mon}} (k_{tcij} + k_{tdij})\mu_{0,i} + (k_{tc\mathrm{Pri}} + k_{td\mathrm{Pri}})C_{P_0} \end{aligned} \tag{20}$$

- Dormant polymer chains with end group j

$$R_{Q_{\mathbf{n},j}} = k_{\mathrm{Cap}Fj}P_{\mathbf{n},j}C_{CAP} - k_{\mathrm{Cap}Rj}Q_{\mathbf{n},j}C_{CAT} + \sum_{i=1}^{N_{mon}}\sum_{\mathbf{m}=\mathbf{0}}^{\infty} k_{cdij}P_{\mathbf{n},j}Q_{\mathbf{m},i} - \sum_{i=1}^{N_{mon}}\sum_{\mathbf{m}=\mathbf{0}}^{\infty} k_{cdji}P_{\mathbf{m},i}Q_{\mathbf{n},j} - k_{decomj}Q_{\mathbf{n},j} \quad (21)$$

- Dead polymer chains

$$R_{D_{\mathbf{n}}} = \sum_{j=1}^{N_{mon}}\left(\alpha_j - \sum_{i=1}^{N_{mon}} k_{tcij}\mu_{0,i}\right)P_{\mathbf{n},j} + \frac{1}{2}\sum_{i=1}^{N_{mon}}\sum_{j=1}^{N_{mon}}\sum_{\mathbf{m}=\boldsymbol{\delta}_\mathbf{i}}^{\mathbf{n}} k_{tcij}P_{\mathbf{m},i}P_{\mathbf{n}-\mathbf{m},j} + \sum_{j=1}^{N_{mon}} k_{decomj}Q_{\mathbf{n},j} \quad (22)$$

- Bulk polymers

$$R_{\sum_{j=1}^{N_{mon}}(P_{\mathbf{n},j}+Q_{\mathbf{n},j})+D_{\mathbf{n}}} = \sum_{j=1}^{N_{mon}}\delta(\mathbf{n}-\boldsymbol{\delta}_\mathbf{j})\left(k_{pj}C_{P_0}C_{Mj} + \sum_{i=1}^{N_{mon}} k_{ctMji}\mu_{0,i}C_{Mj} + x(j)k_{spinij}C_{Mj}^{y(j)}\right) + \sum_{i=1}^{N_{mon}}\sum_{j=1}^{N_{mon}} k_{pji}C_{Mj}P_{\mathbf{n}-\boldsymbol{\delta}_\mathbf{j},i} - \sum_{i=1}^{N_{mon}}\sum_{j=1}^{N_{mon}} k_{pij}C_{Mi}P_{\mathbf{n},j} - \sum_{i=1}^{N_{mon}}\sum_{j=1}^{N_{mon}} k_{tcij}\mu_{0,i}P_{\mathbf{n},j} + \frac{1}{2}\sum_{i=1}^{N_{mon}}\sum_{j=1}^{N_{mon}}\sum_{\mathbf{m}=\boldsymbol{\delta}_\mathbf{i}}^{\mathbf{n}} k_{tcij}P_{\mathbf{m},i}P_{\mathbf{n}-\mathbf{m},j} \quad (23)$$

Moment equations

The moment equations for all polymer species are derived using the moments defined in Table II. By calculating these moments, it is easy to predict polymer properties, such as the number- and weight-average molecular weights and the molecular weight distribution.

- Growing polymer chains

$$\frac{d\mu_{\mathbf{f},j}}{dt} = \delta(\mathbf{n}-\boldsymbol{\delta}_\mathbf{j})^\mathbf{f}\left(k_{pj}C_{P_0}C_{Mj} + \sum_{i=1}^{N_{mon}} k_{ctMji}\mu_{0,i}C_{Mj} + x(j)k_{spinij}C_{Mj}^{y(j)}\right) + \sum_{i=1}^{N_{mon}} k_{pji}C_{Mj}\sum_{\mathbf{a}=0}^{\mathbf{f}}\binom{\mathbf{f}}{\mathbf{a}}\boldsymbol{\delta}_\mathbf{j}^{(\mathbf{f}-\mathbf{a})}\mu_{\mathbf{a},i} - \sum_{i=1}^{N_{mon}} k_{pij}C_{Mi}\mu_{\mathbf{f},j} - \alpha_j\mu_{\mathbf{f},j} - k_{\mathrm{Cap}Fj}C_{CAP}\mu_{f,j} + k_{\mathrm{Cap}Rj}C_{CAT}\nu_{\mathbf{f},j} - \sum_{i=1}^{N_{mon}} k_{cdij}\mu_{\mathbf{f},j}\nu_{0,i} + \sum_{i=1}^{N_{mon}} k_{cdji}\mu_{0,i}\nu_{\mathbf{f},j} \quad (24)$$

- Dormant polymer chains

$$\frac{d\nu_{\mathbf{f},j}}{dt} = k_{\mathrm{Cap}Fj}C_{CAP}\mu_{\mathbf{f},j} - k_{\mathrm{Cap}Rj}C_{CAT}\nu_{\mathbf{f},j} + \sum_{i=1}^{N_{mon}} k_{cdij}\mu_{\mathbf{f},j}\nu_{0,i} - \sum_{i=1}^{N_{mon}} k_{cdji}\mu_{0,i}\nu_{\mathbf{f},j} \quad (25)$$

- Bulk polymers

$$\frac{d\lambda_\mathbf{f}}{dt} = \sum_{j=1}^{N_{mon}}\delta(\mathbf{n}-\boldsymbol{\delta}_\mathbf{j})^\mathbf{f}\left(k_{pj}C_{P_0}C_{Mj} + \sum_{i=1}^{N_{mon}} k_{ctMji}\mu_{0,i}C_{Mj} + x(j)k_{spinij}C_{Mj}^{y(j)}\right) + \sum_{j=1}^{N_{mon}}\sum_{i=1}^{N_{mon}} k_{pji}C_{Mj}\sum_{\mathbf{a}=0}^{\mathbf{f}}\binom{\mathbf{f}}{\mathbf{a}}\boldsymbol{\delta}_\mathbf{j}^{(\mathbf{f}-\mathbf{a})}\mu_{\mathbf{a},i} - \sum_{j=1}^{N_{mon}}\sum_{i=1}^{N_{mon}} k_{pij}C_{Mi}\mu_{\mathbf{f},j} + \frac{1}{2}\sum_{i=1}^{N_{mon}}\sum_{j=1}^{N_{mon}} k_{tcij}\left[\sum_{\mathbf{a}=\mathbf{0}}^{\mathbf{f}}\binom{\mathbf{f}}{\mathbf{a}}\mu_{\mathbf{a},i}\mu_{\mathbf{f}-\mathbf{a},j} - 2\mu_{0,i}\mu_{\mathbf{f},j}\right]$$

These moment equations can be reduced to the leading moment equations as follows:

- Growing polymer chains

  —Zeroth moment, $\mu_{0,_j}$ and μ_0

$$\frac{d\mu_{0,j}}{dt} = k_{pj}C_{P_0}C_{Mj} + \sum_{i=1}^{N_{mon}} k_{ctMji}\mu_{0,i}C_{Mj} + x(j)k_{spinij}C_{Mj}^{y(j)} + \sum_{i=1}^{N_{mon}} k_{pji}C_{Mj}\mu_{0,i} - \sum_{i=1}^{N_{mon}} k_{pij}C_{Mi}\mu_{0,j} - \alpha_j\mu_{0,j} - k_{\mathrm{Cap}Fj}\mu_{0,j}C_{CAP} + k_{\mathrm{Cap}Rj}\nu_{0,j}C_{CAT} - \sum_{i=1}^{N_{mon}} k_{cdij}\mu_{0,j}\nu_{0,i} + \sum_{i=1}^{N_{mon}} k_{cdji}\mu_{0,i}\nu_{0,j} \quad (26)$$

and

$$\frac{d\mu_0}{dt} = \sum_{\mathrm{j}}^{N_{mon}} \frac{d\mu_{0,j}}{dt}$$

Note that $\mu_{0,_j}$ can be simplified as $\mu_{0,_j} = \mu_0 Feg(j)$.

—First moment, $\mu_{\boldsymbol{\delta k},j}$ and $\mu_{\boldsymbol{\delta}_\mathbf{k}}$

$$\frac{d\mu_{\boldsymbol{\delta k},j}}{dt} = \delta(j-k)\left(k_{pj}C_{P_0}C_{Mj} + \sum_{i=1}^{N_{mon}} k_{ctMji}\mu_{0,i}C_{Mj} + x(j)k_{spinij}C_{Mj}^{y(j)}\right) + \sum_{i=1}^{N_{mon}} k_{pji}C_{Mj}\delta(j-k)\mu_{0,i} + \sum_{i=1}^{N_{mon}} k_{pji}C_{Mj}\mu_{\boldsymbol{\delta k},i} - \sum_{i=1}^{N_{mon}} k_{pij}C_{Mi}\mu_{\boldsymbol{\delta k},j} - \alpha_j\mu_{\boldsymbol{\delta k},j} - k_{\mathrm{Cap}Fj}\mu_{\boldsymbol{\delta k},j}C_{CAP} + k_{\mathrm{Cap}Rj}\nu_{\boldsymbol{\delta k},j}C_{CAT} - \sum_{i=1}^{N_{mon}} k_{cdij}\mu_{\boldsymbol{\delta k},j}\nu_{0,i} + \sum_{i=1}^{N_{mon}} k_{cdji}\mu_{0,i}\nu_{\boldsymbol{\delta k},j} \quad (27)$$

and

$$\frac{d\mu_{\boldsymbol{\delta}_\mathbf{k}}}{dt} = \sum_{j=1}^{N_{mon}} \frac{d\mu_{\boldsymbol{\delta k},j}}{dt} = k_{pk}C_{Po}C_{Mk} + \sum_{i=1}^{N_{mon}} k_{ctMki}\mu_{0,i}C_{Mk} + x(k)k_{spinik}C_{Mk}^{y(k)} + \sum_{i=1}^{N_{mon}} k_{pki}C_{Mk}\mu_{0,i} - \sum_{j=1}^{N_{mon}} \alpha_j\mu_{\boldsymbol{\delta k},j} - \sum_{j=1}^{N_{mon}} [k_{\mathrm{cap}Fj}\mu_{\boldsymbol{\delta k},j}C_{CAP} - k_{\mathrm{cap}Rj}\nu_{\boldsymbol{\delta k},j}C_{CAT}] - \sum_{i=1}^{N_{mon}} k_{cdij}\sum_{j=1}^{N_{mon}} \mu_{\boldsymbol{\delta k},j}\nu_{0,i} + \sum_{i=1}^{N_{mon}} k_{cdji}\sum_{j=1}^{N_{mon}} k_{cdji}\mu_{0,i}\nu_{\boldsymbol{\delta k},j} \quad (28)$$

where $\mu_{\boldsymbol{\delta}_\mathbf{k}} = \sum_{j=1}^{N_mon} \mu_{\boldsymbol{\delta}_\mathbf{k}j}$ and $\mu_{\boldsymbol{\delta}_\mathbf{k}j}$ can be simplified as $\mu_{\boldsymbol{\delta}_\mathbf{k}j} = \mu_{\boldsymbol{\delta}_\mathbf{k}} Feg(j)$.

- Dormant polymer chains

—Zeroth moment, $\nu_{0,j}$

$$\frac{d\nu_{0,j}}{dt} = k_{\mathrm{Cap}Fj}\mu_{0,j}C_{CAP} - k_{\mathrm{Cap}Rj}\nu_{0,j}C_{CAT} + \sum_{i=1}^{N_{mon}} k_{cdij}\mu_{0,j}\nu_{0,i} - \sum_{i=1}^{N_{mon}} k_{cdji}\mu_{0,i}\nu_{0,j} \quad (29)$$

—First moment, $\nu_{\boldsymbol{\delta}_\mathbf{k}}, j$ and $\nu_{\boldsymbol{\delta}_\mathbf{k}}$

$$\frac{d\nu_{\boldsymbol{\delta k},j}}{dt} = k_{\mathrm{Cap}Fj}\mu_{\boldsymbol{\delta k},j}C_{CAP} - k_{\mathrm{Cap}Rj}\nu_{\boldsymbol{\delta k},j}C_{CAT} + \sum_{i=1}^{N_{mon}} k_{cdij}\mu_{\boldsymbol{\delta k},j}\nu_{0,i} - \sum_{i=1}^{N_{mon}} k_{cdji}\mu_{0,i}\nu_{\boldsymbol{\delta k},j} \quad (30)$$

and

$$\frac{d\nu_{\boldsymbol{\delta}_\mathbf{k}}}{dt} = \sum_{j=1}^{N_{mon}} [k_{\mathrm{Cap}Fj}\mu_{\boldsymbol{\delta k},j}C_{CAP} - k_{\mathrm{Cap}Rj}\nu_{\boldsymbol{\delta k},j}C_{CAT}] + \sum_{i=1}^{N_{mon}} k_{cdij}\sum_{j=1}^{N_{mon}} \mu_{\boldsymbol{\delta k},j}\nu_{0,i} - \sum_{i=1}^{N_{mon}} k_{cdji}\sum_{j=1}^{N_{mon}} \mu_{0,i}\nu_{\boldsymbol{\delta k},j} \quad (31)$$

- Bulk Polymers

—Zeroth moment, λ_0

$$\frac{d\lambda_0}{dt} = \sum_{j=1}^{N_{mon}} \left(k_{pj}C_{P_0}C_{Mj} + \sum_{i=1}^{N_{mon}} k_{ctMji}\mu_{0,i}C_{Mj} + x(j)k_{spinij}C_{Mj}^{y(j)}\right) - \frac{1}{2}\sum_{i=1}^{N_{mon}}\sum_{j=1}^{N_{mon}} k_{tcij}\mu_{0,i}\mu_{0,j} \quad (32)$$

—First moment, $\lambda_{\boldsymbol{\delta}_\mathbf{k}}$

$$\frac{d\lambda_{\boldsymbol{\delta}_\mathbf{k}}}{dt} = k_{pk}C_{P_0}C_{Mk} + \sum_{i=1}^{N_{mon}} k_{ctMki}\mu_{0,i}C_{Mk} + x(k)k_{spinik}C_{Mk}^{y(k)} + \sum_{i=1}^{N_{mon}} k_{pki}C_{Mk}\mu_{0,i} \quad (33)$$

—Second moment, λ_2

$$\frac{d\lambda_2}{dt} = \sum_{k=1}^{N_{mon}}\sum_{m=1}^{N_{mon}} \frac{d\lambda_{\boldsymbol{\delta}_\mathbf{k}+\boldsymbol{\delta}_\mathbf{m}}}{dt} = \sum_{k=1}^{N_{mon}} \left(k_{pk}C_{P_0}C_{Mk} + \sum_{i=1}^{N_{mon}} k_{ctMki}\mu_{0,i}C_{Mk} + x(k)k_{spinik}C_{Mk}^{y(k)}\right) + \sum_{k=1}^{N_{mon}} \left(\sum_{i=1}^{N_{mon}} k_{pki}C_{Mk}\mu_{0,i} + \sum_{m=1}^{N_{mon}}\sum_{i=1}^{N_{mon}} 2k_{pmi}C_{Mm}\mu_{\boldsymbol{\delta k},i}\right) + \sum_{m=1}^{N_{mon}}\sum_{k=1}^{N_{mon}}\sum_{i=1}^{N_{mon}}\sum_{j=1}^{N_{mon}} k_{tcij}\mu_{\boldsymbol{\delta k},i}\mu_{\boldsymbol{\delta m},j} \quad (34)$$

APPENDIX B: PHYSICAL AND KINETIC PARAMETERS IN THE SIMULATIONS

- Initiator (BPO) decomposition [s^{-1}]: $k_d = 1.7 \times 10^{15}\exp(-30{,}000/RT)$
- Initiator (AIBN) decomposition [s^{-1}]: $k_d = 1.0533 \times 10^{14}\exp(-30{,}704/RT)$

Styrene

Physical parameters

- ρ_M (g/cm^3) = $0.9193 - 6.65 \times 10^{-4}(T - 273.15)$
- ρ_P (g/cm^3) = $0.9926 - 2.65 \times 10^{-4}(T - 273.15)$

Kinetic parameters

- Thermal initiation: k_{spini} (mol^2/L^{-2} / s^{-1}) = $2.19 \times 10^5\exp(-27{,}440.47/RT)$ (Hui et al.[47])
- Propagation: k_p ($L/mol^{-1}/S^{-1}$) = $4.266 \times 10^7\exp(-7769.17/RT)$ (Buback et al.[48])
- Termination: $k_t/k^2_p = 1.1 \times 10^{-5}\exp(12{,}452.2/RT)$ (Hui et al.[47])
- Chain transfer to monomer: $k_{trm}/k_p = 2.198 \times 10^{-1}\exp(-2820/T)$ (Hui et al.[47])
- Gel effect correlation for termination (Hamer et al.[29])

  $g_t = \exp(-0.4404X_P - 6.362X_P^2 - 0.1704X_P^3)$, where $X_P = (C_{M0} - C_M)/C_{M0}$, C_M is the current monomer (plus solvent if there is any) concentrations in the reactor and C_{M0} is the monomer concentration at zero conversion at same reactor conditions.

TEMPO-mediated styrene polymerization

- Forward capping reaction: k_{capf} ($L/mol^{-1}/S^{-1}$) = $5.03 \times 10^9\exp(-3722/RT)$ (Beckwith et al.[38])
- Backward capping reaction: k_{capr} ($1/s$) = $2 \times 10^{13}\exp(-29{,}683/RT)$ (Fukuda et al.[19])
- Thermal decomposition of dormant polymer chains: k_{dec} ($1/s$) = $5.7 \times 10^{14}\exp(-36{,}639.6/RT)$ (Tsujii et al.[40])

n-butyl acrylate

Physical parameters (Beuermann et al.[49])

- ρ_M (g/cm^3) = $0.9211 - 1 \times 10^{-3}(T - 273.15)$
- ρ_P (g/cm^3) = 1.05

Kinetic parameters (Beuermann et al.[49])

- Propagation: k_p ($L/mol^{-1}/S^{-1}$) = $7.37 \times 10^5\exp(-2299/RT)$
- Termination: $k_p/k_t = 2.5 \times 10^{-4}$
- Chain transfer to monomer: $k_{trm}/k_p = 1.3 \times 10^{-4}$

ATRP of styrene and *n*-butyl acrylate at 110°c

- Forward capping reaction for styrene-terminated chains: $k_{capf,1}$ ($L\ mol^{-1}\ S^{-1}$) = 1.15×10^7 (Matyjaszewski et al.[42])
- Backward capping reaction for styrene terminated chains: $k_{capr,1}$ ($L/mol^{-1}/s^{-1}$) = 0.45 (Ohno et al.[50])
- Forward capping reaction for *n*-butyl acrylate–terminated chains: $k_{capf,2}$ ($L/mol^{-1}/s^{-1}$) = 8×10^7. (Note that there is no explicit value reported in the literature. The value chosen here is in the range of forward capping reaction rate constants reported for ATRP using the current catalyst.)
- Backward capping reaction for *n*-butyl acrylate–terminated chains: $k_{capr,2}$ ($L/mol^{-1}/s^{-1}$) = 0.055. (Note that there is no explicit value reported in the literature. The value chosen here is in the range of backward capping reaction rate constants reported for ATRP using the current catalyst.)
- Reactivity ratios: $r_{st} = 0.79$, $r_{BA} = 0.26$ (Brandrup et al.[51])

The cross-termination and chain transfer to monomer rate constants are assumed the same and calculated as a geometrical mean.

- Cross termination: $k_{tc12} = k_{tc21}$ ($L/mol^{-1}/s^{-1}$) = $7.681 \times 10^9\exp(-2690.42/RT)$
- Cross chain transfer to monomer: $k_{trm12} = k_{trm21}$ ($L/mol^{-1}/s^{-1}$) = $2.997 \times 10^4\exp(-7835.8/RT)$

APPENDIX C: INITIATOR EFFICIENCY IN "LIVING" FREE-RADICAL POLYMERIZATION

In a conventional free-radical polymerization, the incorporation of primary radicals produced by thermolysis or photolysis of initiator into polymer chains is usually not 100%. Conversion of primary radicals into effective initiating radicals depends on many factors and typically is not quantitative. The reactions that lead to loss of initiator or initiator-derived radicals include the cage reaction of the initiator-derived radicals, primary radical termination, transfer to initiator, and a variety of other side reactions. The initiator efficiency is defined as the ratio of the total number of primary radicals that initiate polymer chains and the total number of primary radicals that can be provided by the initiator. Note that even in a conventional free-radical polymerization, the initiator efficiency may not be a constant because of its dependency on the reactions mentioned above. The effects of these reactions may vary when the polymerization conditions change and so does the initiator efficiency.

In a "living" free-radical polymerization, when using free stable radicals such as TEMPO in conjunction with conventional initiator, the extra reaction that involves primary radicals is the capping reaction between stable free radicals and primary radicals. It would be of interest to examine how this extra reaction may influence the initiator efficiency. In this research, we do not aim to quantitatively understand how this influence may occur because many kinetic parameters involved in the reactions are still un-

known. Instead, we want to illustrate the general trend of the variation of initiator efficiency, when adding free stable radicals.

Let us consider the following simple scheme shown in Table X. The initiator decomposes to form primary radicals, which experience the primary radical termination, capping reactions with stable free radicals (for simplicity, we use TEMPO here), and propagation to polymer radicals by reacting with monomer. The polymer chain radicals grow by adding more monomer units and experience disproportionation termination. A reversible reaction occurs between polymer chain radicals and free TEMPO to form dormant polymer chains. Note that in this scheme, for the purpose of illustration, we exclude other reactions that lead to the loss of or initiator-derived radicals such as the cage reaction.

The balance equations for this simple system are as follows:

$$\frac{d[I]}{dt} = k_{inid}[I] \tag{35}$$

$$\frac{d[P_0]}{dt} = 2k_{inid}[I] - k_t[P_0]^2 - k_p[P_0][M] - k_{capf}[\text{TEMPO}][P_0] + k_{capr}[\text{TEMPO} - P_0] \tag{36}$$

$$\frac{d\sum_{i=1}^{\infty}[P_n]}{dt} = k_p[P_0][M] - k_{td}\left(\sum_{i=1}^{\infty}[P_n]\right)^2 - k_{capf}[\text{TEMPO}]\sum_{i=1}^{\infty}[P_n] + k_{capr}\sum_{i=1}^{\infty}[\text{TEMPO} - P_n] \tag{37}$$

$$\frac{d\sum_{i=1}^{\infty}[D_n]}{dt} = k_{td}\left(\sum_{i=1}^{\infty}[P_n]\right)^2 \tag{38}$$

TABLE X
Simple Scheme Used to Illustrate the Initiator Efficiency in a "Living" Free-Radical Polymerization System

$I \xrightarrow{k_{inid}} 2P_0$
$2P_0 \xrightarrow{k_t}$ fragments
$P_0 + \text{TEMPO} \overset{k_{cap}}{\rightleftharpoons} \text{TEMPO} - P_0$
$P_0 + M \xrightarrow{k_p} P_1$
$P_n + M \xrightarrow{k_p} P_{n+1}$
$P_n + P_m \xrightarrow{k_{td}} D_n + D_m$
$P_n + \text{TEMPO} \overset{k_{cap}}{\rightleftharpoons} \text{TEMPO} - P_n$

TABLE XI
Kinetic Parameters and Initial Conditions Used to Illustrate the Effect of Addition of TEMPO on Initiator Efficiency

$k_{inid} = 10^{-3}\ \text{s}^{-1}$
$k_t = 10^9\ \text{L mol}^{-1}\ \text{s}^{-1}$
$k_{capf} = 10^9\ \text{L mol}^{-1}\ \text{s}^{-1}$
$k_{capr} = 10^{-1}/\text{s}^{-1}$
$k_p = 1000\ \text{L mol}^{-1}\ \text{s}^{-1}$
$k_{td} = 10^7\ \text{L mol}^{-1}\ \text{s}^{-1}$
$[I]_0 = 0.01\ \text{mol/L}$
$[M]_0 = 10\ \text{mol/L}$

$$\frac{d\sum_{n=1}^{\infty}[\text{TEMPO} - P_n]}{dt} = k_{capf}[\text{TEMPO}]\sum_{i=1}^{\infty}[P_n] - k_{capr}\sum_{n=1}^{\infty}[\text{TEMPO} - P_n] \tag{39}$$

$$\frac{d[\text{TEMPO} - P_0]}{dt} = k_{capf}[\text{TEMPO}][P_0] - k_{capr}[\text{TEMPO} - P_0] \tag{40}$$

$$\frac{d[\text{TEMPO}]}{dt} = -k_{capf}[\text{TEMPO}]\sum_{i=1}^{\infty}[P_n] + k_{capf}\sum_{n=1}^{\infty}[\text{TEMPO} - P_n] - k_{capf}[\text{TEMPO}][P_0] + k_{capr}[\text{TEMPO} - P_0] \tag{41}$$

$$\frac{d[M]}{dt} = -k_p[P_0][M] - k_p\sum_{n=1}^{\infty}[P_n][M] \tag{42}$$

Because we only consider disproportionation termination in this system, each polymer chain consists of one initiator residual at the chain end. The concentration of total polymer chains including the dormant, growing, and dead polymer chains plus the concentration of TEMPO-capped primary species characterize the initiator efficiency when all initiator has been consumed. In the following, let us choose the typical kinetic parameters shown in Table XI, and show how the addition of TEMPO may influence the incorporation of primary radicals into polymer chains. The initial concentrations of initiator and monomer are also shown in Table XI. Figure 25 shows the development of the total concentration of polymer chains plus TEMPO-capped primary species with respect to time for different initial TEMPO concentrations. In the absence of TEMPO, the final concentration of polymer chains is far below the ideal concentration of primary radicals that the initial initiator can provide, which is $2 \times 0.01 = 0.02$ mol/L. However, if increasing the

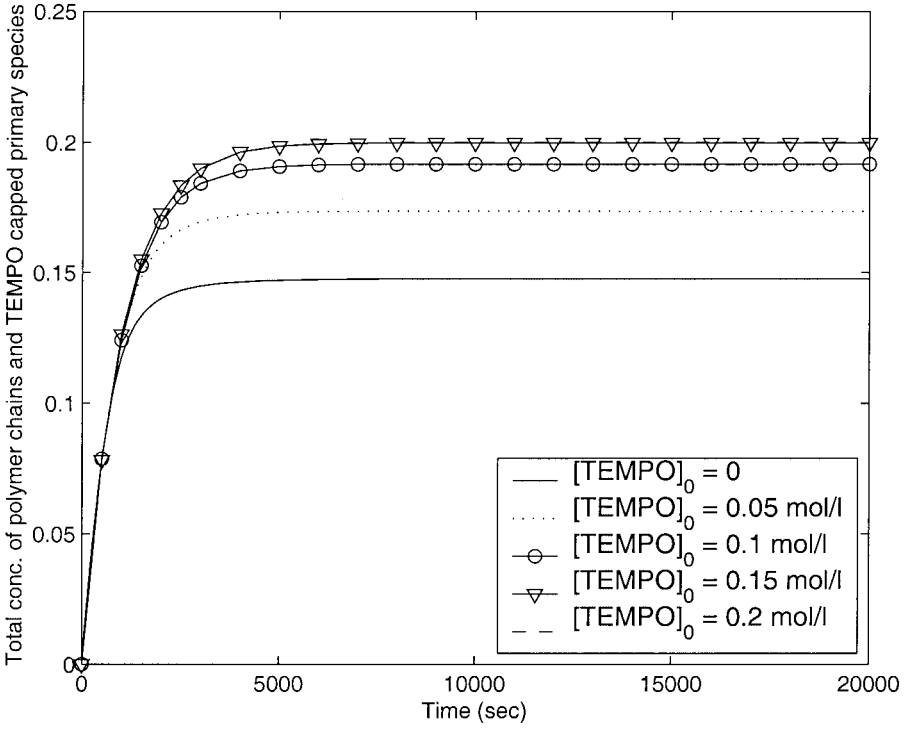

Figure 25 This figure illustrates how the addition of TEMPO may affect the effective number of primary radicals that can initiate polymer chains.

TEMPO concentration, the final concentration of polymer chains plus TEMPO-capped primary species also increases, and thus the initiator efficiency is boosted. A limiting value is reached when the concentration of TEMPO is beyond a certain value because all the primary radicals generated from initiator decomposition are captured by TEMPO.

In summary, through the above example, we believe that the addition of free stable radicals (e.g., TEMPO in combination with a conventional initiator) will boost the conventional initiator efficiency. The same argument can also be applied to thermal initiation of styrene. Using free stable radicals such as TEMPO increases the thermal initiation efficiency, meaning that more radicals generated from thermal initiation will initiate polymer growth compared to a conventional thermally initiated polymerization. However, once the concentration of free stable radicals in the system decreases to a low value, the boost in thermal initiation efficiency disappears.

References

1. Veregin, R. P. N.; Georges, M. K.; Kazmaier, P. M.; Hamer, G. K. Macromolecules 1993, 26, 5316.
2. Mardare, D.; Matyjaszewski, K. Macromolecules 1994, 27, 645.
3. Bon, S. A. F.; Bosveld, M.; Klumperman, B.; German, A. L. Macromolecules 1997, 30, 324.
4. Butté, A.; Storti, G.; Morbidelli, M. Macromolecules 2000, 33, 3485.
5. Holderle, M.; Baumert, M.; Mulhaupt, R. Macromolecules 1997, 30, 3420.
6. Wang, J. S.; Matyjaszewski, K. J Am Chem Soc 1995, 117, 5614.
7. Chong, Y. K.; Le, T. P. T.; Moad, G.; Rizzardo, E.; Thang, S. H. Macromolecules 1999, 32, 2071.
8. Mayadunne, R. T. A.; Rizzardo, E.; Chiefari, J.; Chong, Y. K.; Moad, G.; Thang, S. H. Macromolecules 1999, 32, 6977.
9. Mayadunne, R. T. A.; Rizzardo, E.; Chiefari, J.; Krstina, J.; Moad, G.; Postma, A.; Thang, S. H. Macromolecules 2000 33, 243.
10. deBrouwer, H.; Tsavalas, J. G.; Schork, F. J.; Montiero, M. Macromolecules 2000, 33, 9239.
11. Zhang, M.; Ray, W. H. Ind Eng Chem Res 2001, 40, 4336.
12. Nishikawa, T.; Kamigaito, M.; Sawamoto, M. Macromolecules 1999, 32, 2204.
13. Marestin, C.; Noël, C.; Guyot, A.; Claverie, J. Macromolecules 1998, 31, 4041.
14. Qiu, J.; Gaynor, S. C.; Matyjaszewski, K. Macromolecules 1999 32, 2872.
15. Pan, G.; Sudol, E. D.; Dimonie, V. L.; El-Aasser, M. S. Macromolecules 2001, 34, 481.
16. Yan, D. Y.; Jiang, H.; Fan, X. P. Macromol Theory Simul 1996, 5, 333.
17. Veregin, R. P. N.; Odell, P. G.; Michalak, L. M.; Georges, M. K. Macromolecules 1996, 29, 3346.
18. Greszta, D.; Matyjaszewski, K. Macromolecules 1996, 29, 7661.
19. Fukuda, T.; Terauchi, T.; Goto, A.; Ohno, K.; Tsujii, Y.; Miyamoto, T.; Kobatake, S.; Yamada, B. Macromolecules 1996, 29, 6393.
20. Fischer, H. Macromolecules 1997, 30, 5666.
21. Shipp, D. A.; Matyjaszewski, K. Macromolecules 1999, 32, 2948.
22. Shipp, D. A.; Matyjaszewski, K. Macromolecules 2000, 33, 1553.
23. Ziegler, M. J.; Matyjaszewski, K. Macromolecules 2001, 34, 415.
24. Butté, A.; Storti, G.; Morbidelli, M. Chem Eng Sci 1999, 54, 3225.
25. Zhu, S. P. J Polym Sci Part B: Polym Phys 1999, 37, 2692.
26. He, J. P.; Zhang, H. D.; Chen, J. M.; Yang, Y. L. Macromolecules 1997, 30, 8010.
27. Ray, W. H. J Macromol Sci Rev Macromol Chem 1972, C8, 1.

28. De Gennes, P. G. Scaling Concepts in Polymer Physics; Cornell University Press: Ithaca, NY, 1979.
29. Hamer, J. W. Ph.D. Thesis, University of Wisconsin at Madison, 1983.
30. Devonport, W.; Michalak, L.; Malmstrom, E.; Mate, M.; Kurdi, B.; Hawker, C. J.; Barclay, G. C.; Sinta, R. Macromolecules 1997, 30, 1929.
31. Goto, A.; Fukuda, T. Macromolecules 1997, 30, 4272.
32. Veregin, R. P. N.; Odell, P. G.; Michalak, L. M.; Georges, M. K. Macromolecules 1996, 29, 4161.
33. Veregin, R. P. N.; Odell, P. G.; Michalak, L. M.; Georges, M. K. Macromolecules 1996, 29, 2746.
34. Yoshida, E.; Tanimoto, S. Macromolecules 1997, 30, 4018.
35. Rizzardo, E. Chem Aust 1987, 54, 32.
36. Solomon, D. H.; Rizzardo, E.; Cacioli, P. U.S. Pat. 4,581,429, 1986.
37. Zhang, M. Ph.D. Thesis, University of Wisconsin at Madison, 2001.
38. Beckwith, A. L. J.; Bowry, V. W.; Ingold, K. H. J Am Chem Soc 1992, 114, 4983.
39. Skene, W. G.; Scaiano, J. C.; Listigovers, N. A.; Kazmaier, P. M.; Georges, M. K. Macromolecules 2000, 33, 5065.
40. Tsujii, Y.; Kukuda, T.; Miyamoto, T. Polym Prepr (Am Chem Soc Div Polym Chem) 1997, 38, 657.
41. Arehart, S. V.; Matyjaszewski, K. Macromolecules 1999, 32, 2221.
42. Matyjaszewski, K.; Patten, T. E.; Xia, J. H. J Am Chem Soc 1997, 119, 674.
43. Hawker, C. J.; Barclay, G. G.; Orellana, A.; Dao, J.; Devonport, W. Macromolecules 1996, 29, 5245.
44. Patten, T. E.; Matyjaszewski, K. Acc Chem Res 1999, 32, 895.
45. Arehart, S. V.; Greszta, D.; Matyjaszewski, K. Polym Prepr (Am Chem Soc Div Polym Chem) 1997, 38, 705.
46. Greszta, D.; Matyjaszewski, K.; Pakula, T. Polym Prepr (Am Chem Soc Div Polym Chem) 1997, 38, 709.
47. Hui, A. W.; Hamielec, A. E. J Appl Polym Sci 1976, 16, 749.
48. Buback, M.; Gilbert, R. G.; Hutchinson, R. A.; Klumperman, B.; Kuchta, F.; Manders, B. G.; O'Driscoll, K. F.; Russell, G. T.; Schweer, J. Macromol Chem Phys 1995, 196, 3267.
49. Beuermann, S., Jr.; Paquet, D. A.; McMinn, J. H.; Hutchinson, R. A. Macromolecules 1996, 29, 4206.
50. Ohon, K.; Goto, A.; Fukuda, T.; Xia, J. H.; Matyjaszewski, K. Macromolecules 1998, 31, 2699.
51. Brandrup, J.; Immergut, E.; Grulke, E., Eds. Polymer Handbook, 4th ed.; Wiley: New York, 1999.